HELSINKI UNIVERSITY OF TECHNOLOGY
Faculty of Electronics, Communications and Automation

Zhong Zheng

ON THE FEMTOCELL CONCEPT: PERFORMANCE STUDIES AND APPLICATION IN THE PUBIC SAFETY FRAMEWORK

Thesis submitted for examination for the degree of Master of Science in Technology

Espoo 20.12.2009

Thesis supervisor:

Prof. Jyri Hämäläinen

Thesis instructor:

M.Sc. Mika Husso, Dr. Edward Mutafungwa

Author: Zhong Zheng

Title: On the Femtocell concept: performance studies and application in the Pubic Safety framework

Date: 20.12.2009 Language: English Number of pages: 10+76

Faculty: Faculty of Electronics, Communications and Automation

Professorship: Communication engineering Code: S-72

Supervisor: Prof. Jyri Hämäläinen

Instructor: M.Sc. Mika Husso, Dr. Edward Mutafungwa

3G femtocell is a small base station operating on UMTS spectrum with low manufacturing cost. It creates a small hotspot with a radio coverage area at order of tens square meters. At a reduced distance between transmitter and receiver, the transmission power of terminal is lowered and thus, it reduces the average radio interference power level and uses the spectrum more efficiently. The traffic backhaul is carried out by wireline Internet connection between subscriber premises and mobile operator's core network. The femtocell concept provides an efficient solution to extend the mobile radio coverage area indoors, especially at homes.
However, as the femtocell devices are owned and deployed by users, we face an uncoordinated cell configurations. The spectrum reuse distance can be arbitrarily small and inter-cell interference cannot be controlled by dedicated cell planning.
This thesis will discuss the the status of current standardization of femtocell in 3GPP and evaluate the possible technical problems in femtocell rollout. We will study the femtocell interference scenarios in a simplified dwelling environment make an analysis of the impacts on femtocell performance due to building structure and configuration parameters. Performance of femtocells was examined by system level simulations.
A case study on femtocell application in mobile teletrauma service will be investigated. In this use case, being complementary with macrocellular network, the femtocell is used as an indoor access point to carry out rich medical multimedia service between emergency site and remote consulting expert. The medical data assists the consultants to participate in the treatment and decision-making procedure.
In addition, we propose and analyze a method based on beamforming technique where terminals may have a control-only connection to adjacent femtocell for interference mitigation purposes. It is found that even simple multiantenna methods can be effectively used to suppress co-channel interference.

Keywords: Femtocell, WCDMA, HSPA, public safety, beamforming, interference suppression

Preface

This thesis was part of the CHI-FIN UBI-SERV project[1] carried out from 2009. It was written in the Department of Communication and Networking at Helsinki University of Technology.

Firstly, I would like to thank Professor Jyri Hämäläinen for being my supervisor and giving me invaluable guidance and teaching to finish this thesis. I also would like to thank my instructors Mika Husso and Edward Mutafungwa for their support and generous sharing in empirical knowledge. Most of all, I would like to express my gratitude to all my colleagues in the department for their assistance.

Also, I would like to express my gratitude to my girl friend Chunfang Tang for her love and continuous support.

Finally, I am deeply and forever obliged to my family for their love, support and encouragement throughout my entire life.

Otaniemi, 20.11.2009

Zhong Zheng

[1]User-centric Design of Ubiquitous Welfare and Safety Services and Supporting Technologies for China and Finland (CHI-FIN UBI-SERV). It is funded by Academy of Finland: `http://www.ubi-serv.org/`

Contents

List of Figures

List of Tables

List of Abbreviations

2G	2nd Generation
3G	3rd Generation
3GPP	3rd Generation Partnership Project
ATM	Asynchronous Transfer Mode
AWGN	Additive White Gaussian Noise
BMC	Broadcast/Multicast Control
BPSK	Binary Phase-Shift Keying
CCTrCh	Coded Composite Transport Channel
CN	Core Network
CRC	Cyclic Redundancy Check
CSG	Close Subscriber Group
DSL	Digital Subscriber Line
E-DCH	Enhanced Dedicate Channel
EMP	Emergency Medical Paramedics
FDMA	Frequency Division Multiple Access
GPS	Global Positioning System
GSM	Global System for Mobile communications
HARQ	Hybrid Automatic Repeat Request
HNB	Home NodeB
HNB-GW	Home NodeB Gateway
HS-DSCH	High-Speed Downlink-Shared Channel

HSPA	High Speed Packet Access
IMT-2000	International Mobile Telecommunications-2000
IP	Internet Protocol
IS-95	Interim Standard 95
ITU	International Telecommunication Union
MAC	Medium Access Control
MDU	Multiple Dwelling Unit
OVSF	Orthogonal Variable Spreading Factor
PDCP	Packet Data Convergence Protocol
QoS	Quality of Service
RAB	Radio Access Bearer
RLC	Radio Link Control
RNC	Radio Network Controller
RRC	Radio Resource Control
RRM	Radio Resource Management
SeGW	Security Gateway
TDMA	Time Division Multiple Access
TFC	Transport Format Combination
TTI	Transmit Time Interval
UE	User Equipment
UMTS	Universal Mobile Telecommunications System
UTRAN	UMTS Terrestrial Radio Access Network
WCDMA	Wideband Code Division Multiple Access

Chapter 1

Introduction

Femtocell base station (FBS), also denoted as Home NodeB (HNB) in 3GPP specification, is known as a nomadic base station with very low transmission power and low manufacturing cost. It is usually placed indoors and it provides dedicated access for 4–6 indoor users that belong to a Close Subscriber Group (CSG). It looks very much like a WLAN access point as depicted in Fig. 1.1, but unlike Wi-Fi it utilizes existing Universal Mobile Telecommunication System (UMTS) radio interface and radio transmission is carried out on a licensed spectrum. The data packages to FBS are routed through wireline broadband connection that is established between user premises and mobile operator's core network.

The mobile networks coverage is relatively good in many developed countries, but still, even in urban regions, there are always areas where radio signal is difficult to reach due to the challenging of geographical topology or building heavy construction materials. Situation is worse in the currently deployed UMTS networks than in 2G since UMTS operates at higher frequency band and thus signal does not penetrate inside buildings as effectively as signals does in 2G system [1]. Instead of deploying more Macrocell Base Stations (MBSs) to fill up indoor coverage holes, FBS is a better indoor coverage solution. It is more spectral efficient to use femtocells, because building walls can well separate the radio propagation between indoor femtocells and macrocells. In addition, outer wall attenuation together with intrinsic short communication distance within a femtocell, will keep transmission power of both FBS and femtocell user equipment (FUE) at a low level while maintain a high data rate.

The recently introduced 3.5G technology updates has raised the radio capacity to a new level and data rates are closing to usual DSL connection rates. The network capacity in cellular technologies, however, is shared by all users within the cell area and therefore individual users see a fluctuated data rate depending on the number of active users. As the demands for broadband mobile connection increase, the huge need for quick capacity improvement has been absorbed. However, previous studies show that a majority of mobile phone usage take place at home [2]. Therefore, by a massive femtocell deployment, indoor users will have a better service experience and there will be a significant traffic offloading from macrocell networks, which gives additional macrocell capacity gains. This helps the operators to concentrate on the real mobile demands and to provide improvement on services due to better return of investments.

Recent studies have shown promising results for femtocell indoor coverage as well as high data throughputs. Home cells give new opportunity for indoor UMTS service provision and they may become a technological enabler for many broadband services deployed within mobile network infrastructure. As an example, this thesis considers a femtocell use case where pre-hospital Medical Emergency Care (MEC) service is provided by remote surgical consultants through mobile network to the on-site emergency medical paramedics (EMPs) [3]. At the emergency site that is usually patient's apartment/house, the multimedia medical telemetry can be constantly monitored by remote experts and videoconferencing is carried out to promptly guide emergency care actions. To provide the aforementioned services based on UMTS networks, it is crucial to maintain a reliable channel in an indoor environment with a data rate up to 1Mbps. Thus, to show benefits that femtocells promise due to improved coverage and throughput, this thesis presents the MEC service provision by means of hybrid macro- and femtocellular networks.

This thesis will focus on the femtocellular interference analysis and propose a femtocell case study on MEC service provision. Chapter 2 introduces the concept of WCDMA technology and describes radio network architectures and protocols of UMTS and High Speed Packet Access (HSPA). Chapter 3 gives the overview of femtocell framework and introduces related technical challenges to incorporate femtocell into existing infrastructure, followed by a presentation of system model used

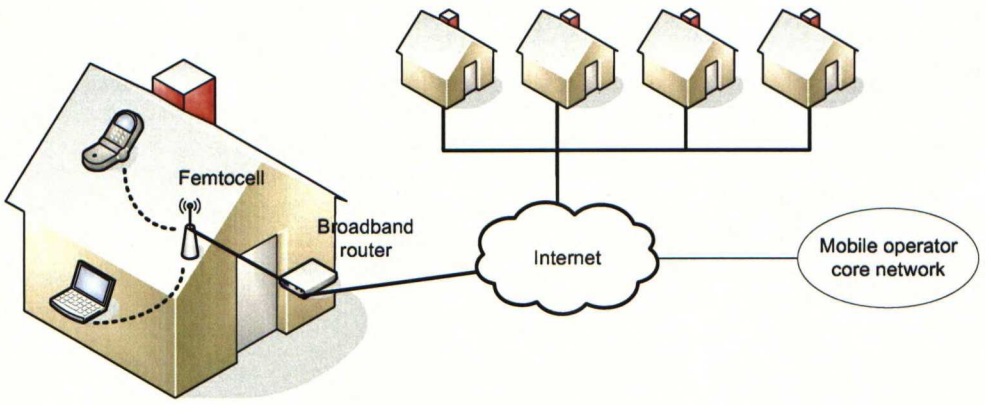

Figure 1.1: Femtocell concept

in system simulations. In addition, it prompts a femtocell solution that is used to provide indoor MEC service in a multiple dwelling units (MDUs). Chapter 4 discusses the operational parameters of femtocell and shows simulation results on both femtocell performance and MEC service provision. Chapter 5 proposes a novel collaborative beamforming method to suppress downlink interference from FBS to neighboring FUEs. It also presents the analytical model and performance measurement result. Chapter 6 summarizes the thesis.

Chapter 2

UMTS radio interface architecture

In 3GPP specification UMTS system consists of UMTS Terrestrial Radio Access Network (UTRAN) domain and Core Network (CN) domain. Logical network elements are grouped into these 2 domains based on their functionalities. According to 3GPP specifications, both User Equipment (UE) and UTRAN elements contains a set of protocols which are introduced to cater the need required by WCDMA and HSPA technologies. Yet, CN preserves the protocol stack from GSM system so as to naturally evolve from existing system while having new radio capability. The framework of this thesis assumes the network and protocol architecture of UTRAN.

Fig. 2.1 shows a schedule of UMTS standards evolution. In 3GPP Release 99, WCDMA was designed to provide flexible data rates and integration of various services by a single radio interface without particular optimization. Compared with 2G system, WCDMA is featured with up to 384kbps practical data rate in both uplink and downlink, low packet latency and simultaneous voice and packet data capability. In Release 5 and 6, the radio interface capacities were further boosted by implementing HSDPA and HSUPA in the existing networks and terminals. Thanks to extensive multi-codes, fast Layer 1 HARQ and physical layer scheduler, the data rate was enhanced up to 14.4Mbps in downlink and 5.76Mbps in uplink.

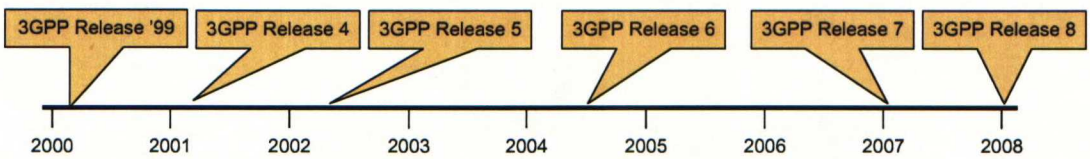

Figure 2.1: WCDMA evolution timeline in 3GPP standardization process

This chapter gives an overview of UTRAN architecture, including an introduction to WCDMA technology, system and protocol frameworks of UTRAN. Network changes due to HSPA evolution are also explained.

2.1 WCDMA basics

Originally CDMA technology was developed and used for military proposes during the World War II. It allows the received signal to be hidden below the noise level while applying the so-called spread spectrum procedure. Few decades ago it was shown that the interference suppression feature of CDMA provides a many-fold capacity gain over competing technologies and the CDMA concept was drawn an interest in civil mobile phone market [4]. In 1993 first IS-95 cellular network was deployed in USA and it was the first commercial cellular system that used CDMA in its radio interface. During the IMT-2000 progress which aims to create mobile communication technology framework, Wideband CDMA (WCDMA) was proposed to ITU by 3GPP. Both of IS-95 and WCDMA are Direct-sequence CDMA (DS-CDMA) systems, where each original bit in user data stream is replaced by an assigned chip code, resulting in increased data rate and bandwidth.

The wideband property of WCDMA reflects on its 3.84Mcps chip rate that enables higher bit rate, in comparison with 1.2288Mcps in IS-95. In addition, higher chip rate allows the system to utilize multi-path diversity by Rake receiver to improve system performance and coverage. It is also worth of mentioning that IS-95 has synchronized cells and synchronization reference signal is usually provided by the Global Positioning System (GPS). This makes it difficult to deploy indoor cell where GPS signal can be hardly reach [5]. In contrast to IS-95, WCDMA system is designed to be asynchronous without the need of GPS reception. Other parameters are compared in Table 2.1.

From a radio resource usage perspective, CDMA allocates resources more efficiently than FDMA or TDMA which allocate orthogonal bandwidths and timeslots to users. In practical systems, a guard band in FDMA is needed between adjacent bands to avoid inter-user interference in case of frequency error due to Doppler shift. Similarly, a guard interval is needed in TDMA system due to synchronization errors.

Table 2.1: Radio link parameter comparison between WCDMA and IS-95

	WCDMA	IS-95
Bandwidth	5MHz	1.25MHz
Chip rate	3.84Mcps	1.2288Mcps
Base station synchronization	No	Yes
Power control frequency	1500Hz in both uplink and downlink	800Hz in uplink, slow power control in downlink

Unlike the aforementioned technologies, CDMA uses a set of orthogonal chip codes to separate parallel radio transmissions and allows users to fully utilize all the resources simultaneously.

Fig. 2.2 depicts the spreading and despreading principles of DS-CDMA. Without loss of generality, we assume in Fig. 2.2 the original user data bits are BPSK modulated and bit rate is R with a occupying bandwidth proportional with R. In each bit duration $T = 1/R$, the original bit is multiplied with a BPSK-modulated chip code with chip interval $T_c = T/SF$, where SF is the spreading factor. In this example, the bit rate of resulted data stream is increased to $8R$ with a $SF = 8$. Correspondingly, new data stream occupies a extended bandwidth proportional with $8R$.

The detected bits sequence in the receiver is multiplied with the same chip code as that in its spreading procedure. The multiplication of chip code and desired bit sequence is done bitwise and it recovers exactly the same user bits, provided that chip code is perfectly synchronized with spreaded bit sequence. In contrary, other bits with different spreading codes produce a random-like sequence after the despreading procedure. Then, while integrating signal over duration T, the desired signal amplitude is raised on average by an amplitude of SF over the interference from other users. Interference from other transmission with different spreading codes is suppressed down to a level that depends on the cross-correlation between spreading codes.

The desired user signal is detected out of simultaneous user transmissions by implementing a code correlator at receiver end. The received signal at receiver d is a sum

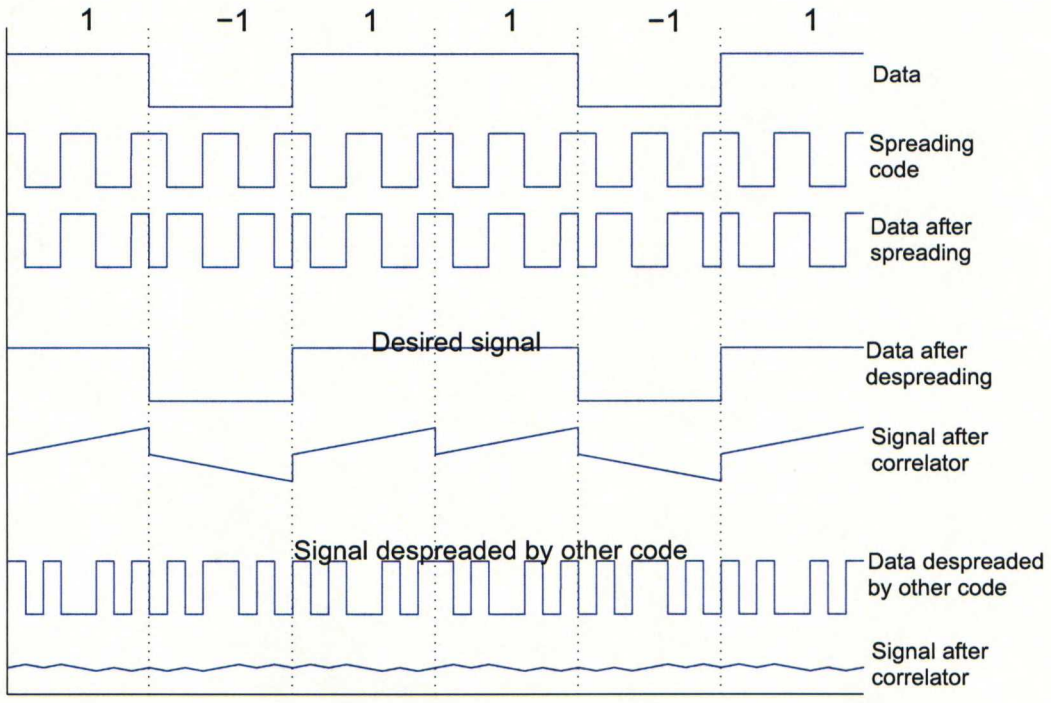

Figure 2.2: Spreading and despreading principle

of all active N users' signals within the same frequency band and is given by

$$\mathbf{r_d} = \sum_{i=1}^{N} h_i s_i \mathbf{c_i} + \mathbf{n}, \tag{2.1}$$

where s_i and $\mathbf{c_i}$ are user bit and its corresponding chip code of user i, h_i is the channel amplitude experienced by user i and it is assumed to be constant during the chip code interval, $\mathbf{n}$ is white Gaussian noise seen by the receiver. The signal stream is then correlated with the identical chip code $\mathbf{c_d}$ as that in spreading procedure of transmitter d

$$\begin{aligned} z_d &= \mathbf{c_d^T} \cdot \mathbf{r_d} \\ &= h_d s_d \mathbf{c_d^T} \cdot \mathbf{c_d} + \sum_{i=1}^{N, i \neq d} h_i s_i \mathbf{c_d^T} \cdot \mathbf{c_i} + \mathbf{c_d^T} \cdot \mathbf{n} \\ &= h_d s_d x_d + \sum_{i=1}^{N, i \neq d} h_i s_i x_i + \mathbf{c_d^T} \cdot \mathbf{n}, \end{aligned} \tag{2.2}$$

where $\mathbf{c_d^T}$ is the transpose of chip code from user d. The chip code auto-correlation

Table 2.2: Functionalities of spreading and scrambling codes

	Spreading code	Scrambling code
Propose	Separation of different physical channels from a single source	**Uplink:** separation of different terminals. **Downlink:** separation of different base stations
Code family	OVSF	Long 10ms code: Gold code Short 66.7μs code: Extended S(2) code
Orthogonality	Orthogonal codes	Pseudo-random codes
Spreading	Yes	No

x_d and cross-correlation x_i are given as below

$$x_d = \mathbf{c_d^T} \cdot \mathbf{c_d}, \tag{2.3}$$

$$x_i = \mathbf{c_d^T} \cdot \mathbf{c_i}. \tag{2.4}$$

With coherent detection, the post-processing signal-to-interference plus noise ratio (SINR) after despreading at receiver d, also denoted as $(E_b/N_0)_d$, is formulated as

$$\begin{aligned}(E_b/N_0)_d &= \frac{|h_d|^2|s_d|^2|x_d|^2}{\sum_{i=1}^{N,i\neq d}|h_i|^2|s_i|^2|x_i|^2 + \mathbb{E}\{\mathbf{c_d^T n n^H c_d}\}} \\ &= \frac{|x_d|^2 P_{RX}^d}{\sum_{i=1}^{N,i\neq d}|x_i|^2 P_{RX}^i + x_d N_0},\end{aligned} \tag{2.5}$$

where $P_{RX}^i = |h_i|^2|s_i|^2$ is the received signal power from user i. Thus, the detection performance of DS-CDMA depends greatly on the auto- and cross-correlation properties of spreading codes.

2.2 Channelization and scrambling codes

In WCDMA system, there are two types of codes involved in the transmission procedure, namely channelization code and scrambling code. The functionalities of these 2 codes are summarized in Table 2.2.

Channelization codes are designed to separate different physical transmissions from a single source, i.e. physical channels from one UE in uplink or from one base station in downlink. Because synchronization can be always maintained between channels originating from one source, WCDMA uses orthogonal code set in the

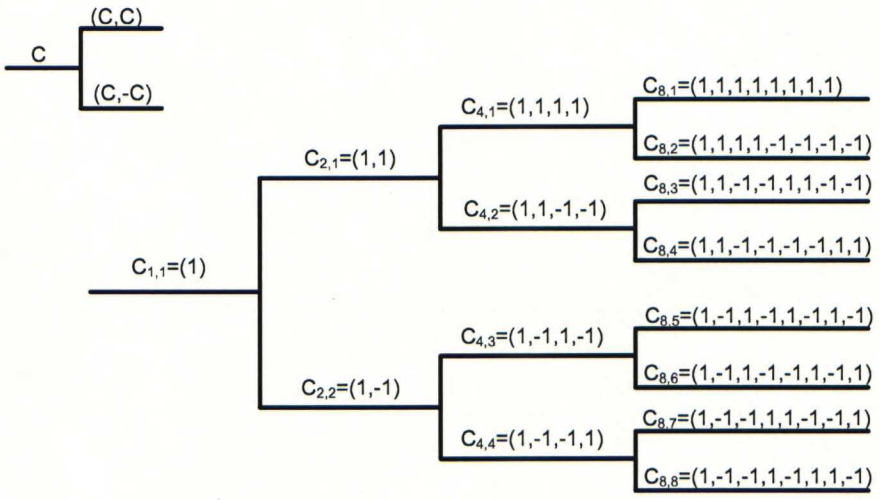

Figure 2.3: Channelization code tree

spreading procedure to maximize the ratio between code auto- and cross-correlation. As depicted in (2.3) and (2.4), when orthogonal codes are used, the auto-correlation is given as $\mathbf{c_d^T} \cdot \mathbf{c_d} = SF^2$ and cross-correlation is 0, provided that there is no time delay (t=0) in this operation. The resulting $(E_b/N_0)_d$ is then

$$(E_b/N_0)_d = SF\frac{P_{RX}^d}{N_0}, \tag{2.6}$$

where the interference from other transmissions completely disappear due to the orthogonality between codes.

The channelization code set is constructed based on the Orthogonal Variable Spreading Factor (OVSF) technique. OVSF is able to combine messages with different spreading factors and keep orthogonality between them, which enables the flexibility to choose service data rate and services integration. As illustrated in Fig. 2.3, the code tree is generated as follows: the codes with spreading factor N are generated by repeating the code c with spreading factor $N/2$ in the form of $\{c, c\}$ and $\{c, -c\}$ [6].

There are some restrictions in use of OVSF code tree for the channelization code selection. Restrictions are due to orthogonality requirement between codes in parallel usage. If a certain code in the code tree is reserved for a physical layer transmission, none of the codes in the underlying branches of the same code tree can be used.

Because of asynchronous operation in WCDMA, the orthogonality of codes used by

different sources cannot be maintained due to arbitrary time offset. In asynchronous operations the orthogonal code set leads to a bad performance in both auto- and cross-correlation. By contrast, any two codes from a random code set have a expected cross-correlation x_i equal to square-root of code length SF. When random code set is used, the $(E_b/N_0)_d$ is formulated as

$$(E_b/N_0)_d = \frac{SF^2 P_{SF}^d}{\sum_{i=1}^{N,i\neq d} SF P_{RX}^i + SF N_0} = SF \frac{P_{RX}^d}{\sum_{i=1}^{N,i\neq d} P_{SF}^i + N_0}. \quad (2.7)$$

Thus, in addition to use channelization codes, a scrambling operation is carried out in each transmitter to randomize the chip codes. By suppressing the cross-correlation, scrambling code aims to separate transmissions from different sources. It separates transmission from different UEs in uplink and transmissions from different base stations in downlink. In contrary to channelization code, the length of scrambling code is equal to the size of transmission block. Thus, a scrambling code does not change the transmission bandwidth. In uplink, scrambling operation uses either a Gold code of 38400 chips that corresponds to a 10ms transmission block or a short code from Extended S(2) code family with 256 chips. In downlink, system uses long codes and the same Gold code as in uplink [6].

2.3 UTRAN network architecture

UTRAN is a transport medium that inter-connects mobile user and operator core network infrastructure. It creates and maintains Radio Access Bearers (RABs), which transport user data and control signaling transparently between UE and CN. Utilizing RABs service, CN elements obtain a communication path towards UE without a need to be involved in radio access aspect. This is a major design criteria in UTRAN as CN is acquired directly from the GSM networks [7]. During the procedure of RAB establishment, the QoS requirements that are negotiated between UE and CN are mapped to the parameter configuration of target RAB by UTRAN.

Fig. 2.4 depicts the architecture of UTRAN networks. The inter-connection formats between logical elements are defined as open interfaces by which devices from different vendors can inter-operate. UTRAN contains entities that are located between Uu and Iu interfaces. It consists of a group of logical elements which enable the

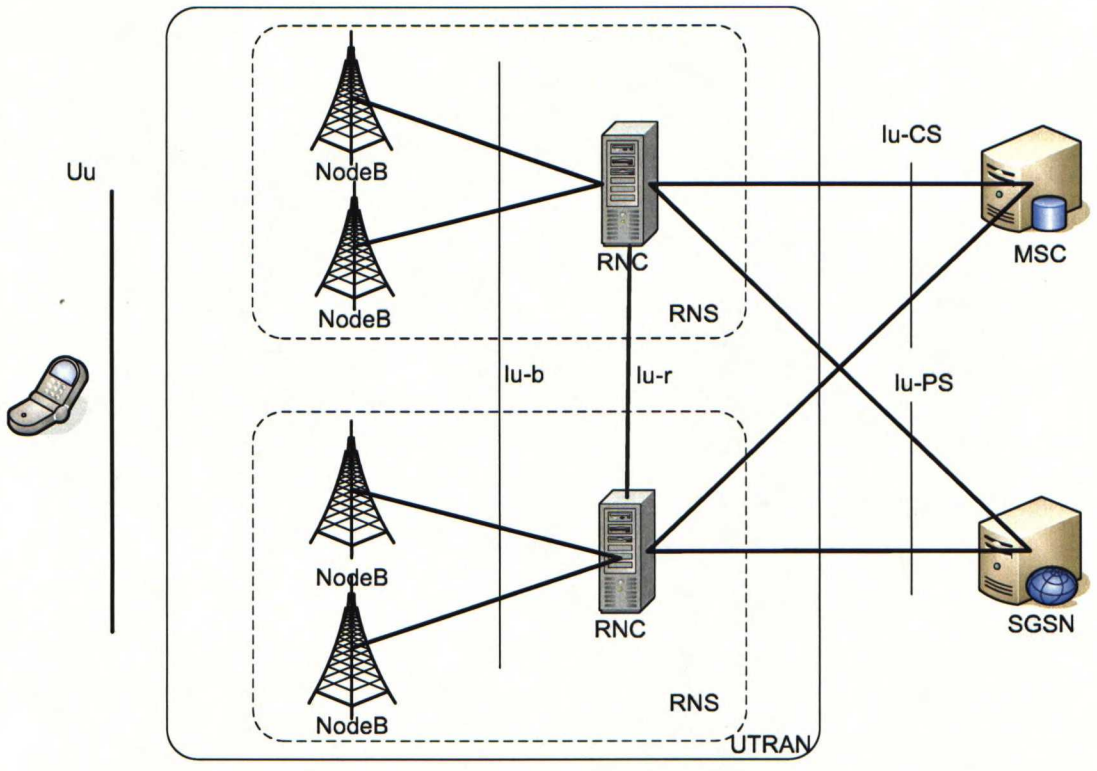

Figure 2.4: UTRAN network architecture

wireless connectivity for users. In addition, it carries out Radio Resource Management (RRM) and mobility management functions for UEs. UTRAN contains one or more NodeBs that logically correspond to base stations in GSM terminology, and their controlling Radio Network Controller (RNC) that corresponds to base station controller in GSM. The NodeBs together with their direct controlling RNC constitute a Radio Network Sub-system (RNS) in UTRAN. There can be one or more RNSs in one UTRAN. The physical transport between UTRAN logical elements is encapsulated as an alternative module. It uses Asynchronous Transfer Mode (ATM) in Release 99 and allows Internet Protocol (IP) based transport from Release 5 onwards.

The NodeB provides the first interface between mobile user and fixed networks and it utilizes WCDMA technology in Release 99 compliance networks. With a common Uu interface, it provides for mobile users the RABs services, which include data services in both CS and PS domain, and radio access signaling from or to users. It also carries data and control transport channels through Iub interface

to its controlling RNC and receives configuration signaling. The main function of NodeB is to carry out air interface processing in Layer 1, which includes user data spreading, channel coding and modulation, data rate adaption, etc. It translates and fits the data streams and higher layer control information into radio frame and performs radio signal reception and transmission operations. In addition, it is partly involved in RRM as fast close-loop power control is carried out by NodeB.

The RNC is the network element responsible for switching and controlling in UTRAN networks. It is located between Iub and Iu interfaces, and has third interface Iur for inter-connection with other RNCs. RNC may have two logical roles in a communication path from UE to CN depending on whether it terminates the Iu interface or not. As depicted in Fig. 2.5, the Service RNC (SRNC) is logically located at the end of a communication path in UTRAN and provides Iu bearer service in cooperation with CN. It also terminates the Radio Resource Control (RRC) protocol between UE and UTRAN. SRNC performs the signal processing in Layer 2, including basic RRM, parameter mapping between transport channels and physical channels, for example. In addition, Drift RNC (DRNC) concept is created due to the soft handover technique used in UTRAN. DRNC terminates the physical layer processing of RAB and forwards data transparently to SRNC through Iur interface. There could be zero, one or more DRNCs with respect to a UE. In SRNC macrodiversity gain can be achieved by combining data streams from DRNCs and SRNC.

The main responsibility of RNC is to carry out RRM operation to establish and maintain radio services with fulfilled QoS requirements. The RRM operations include a group of algorithms that are needed to deliver control information over radio path between UE and UTRAN. The control signaling is conveyed by RRC protocol. The RRM algorithms include the following procedures that are important for this work:

- Handover control. Handover is an essential procedure to guarantee user mobility and connectivity throughout entire cellular networks. It ensures that the on-going phone call or data session is transfered from current cell to another, when the subscriber moves from the coverage area of a current cell to that of target cell or when the traffic load of current cell needs to be off-loaded. As illustrated in Fig. 2.6, there are three types of handover defined in UTRAN:

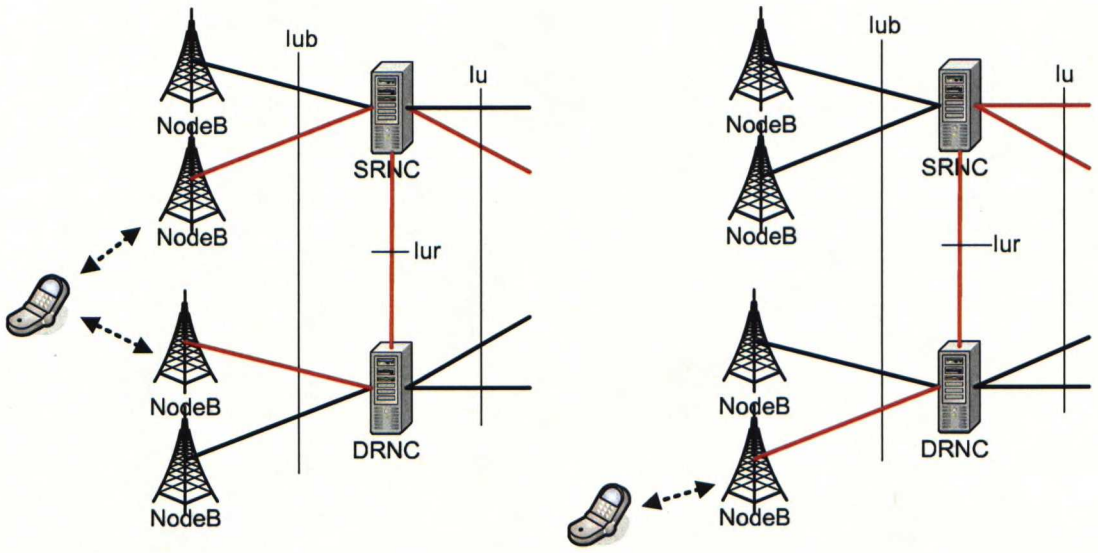

Figure 2.5: Logical role of the RNC for one UE UTRAN connection

hard handover, soft handover and softer handover. Hard handover occurs if the old radio connection with current cell is released before new connection is established. Thus, there is only one communication path maintained between UE and SRNC and user's session will experience a very short break which is usually not visible for a user. Hard handover can be used in intra- and inter-frequency handover depending on whether the frequency band of new channel is the same as that of the old channel. If multiple frequency bands are deployed in network, inter-frequency hard handover can be carried out. It may efficiently reduce the co-channel interference in densely populated area like in urban center. In addition, when multiple bands are deployed as a hierarchic structure such as two-tier macro- and microcell, inter-frequency handover can reduce the amount of signaling traffic by switching user to macrocell band when he/she transverses rapidly across a large area [5].

Soft and softer handover are important features implemented in UTRAN. Unlike hard handover, they allow mobile user to have simultaneous radio connection with different cells (soft handover) or sectors that belong to the same BS (softer handover). In downlink additional capacity is consumed due to duplicated data stream transmissions, but in uplink the macrodiversity gain is achieved and interference from mobile user to neighboring cells is reduced.

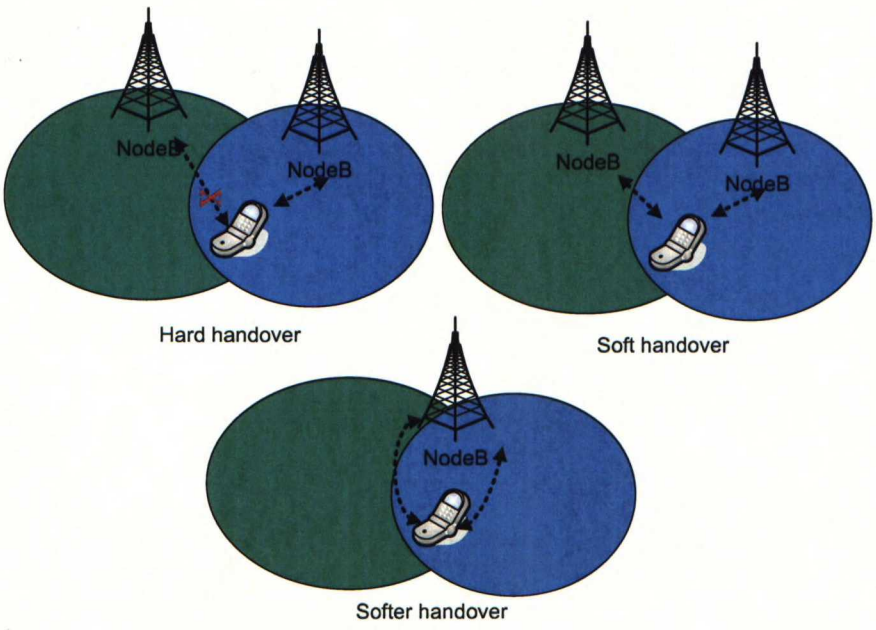

Figure 2.6: Handovers in UTRAN

- Power control. In order to reduce the co-channel interference, power control is carried out to find proper transmission power level in terminals. In uplink power control is especially needed to overcome the near-far problem. Because of asynchronous operation mode of UTRAN, the physical transmissions from different sources are non-orthogonal and they interfere with each other according to (2.7). If there is no power control mechanism, in uplink the UE that is located nearby its serving BS may dominate the base station receiving power and block the other radio transmissions within the entire cell. Thus, the uplink power control in WCDMA is designed to keep the transmission power of UEs at the minimum while maintaining the received power at the BS that is required to fulfill the QoS requirement. Uplink power control applies a closed-loop control between UE and NodeB which keeps the received SINR value variations feasible, and an open-loop control between NodeB and RNC which sets the target SINR value that is needed by the service.

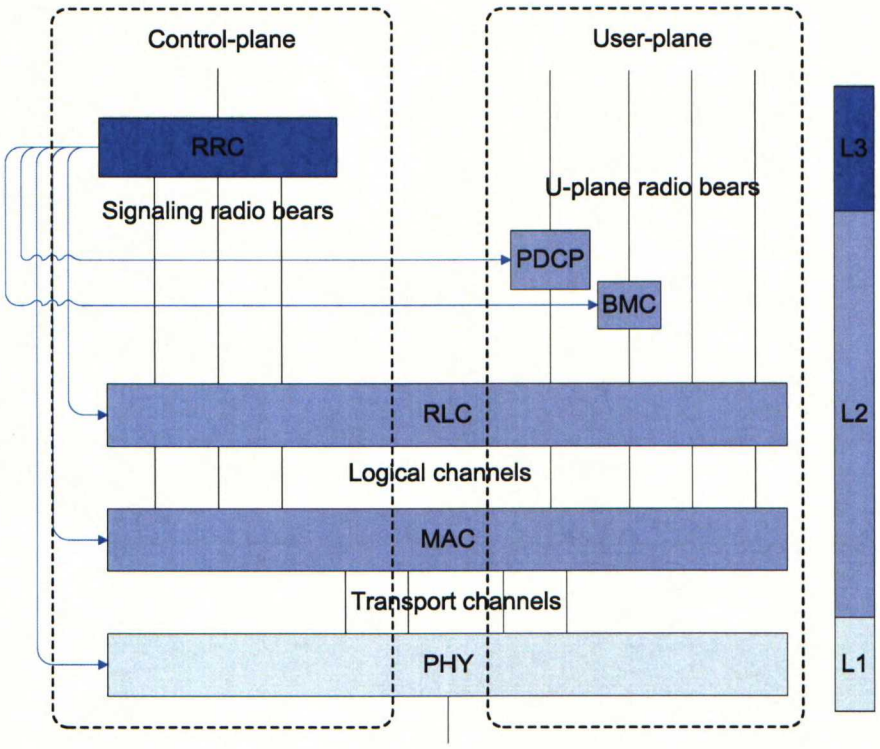

Figure 2.7: UTRA FDD radio interface protocol architecture

2.4 Radio interface protocol architecture

Radio interface protocols are designed to set up, reconfigure, and release Radio Bearer (RB) services, which are used by mobile user and NodeB. Fig. 2.7 shows the radio interface protocol architecture. The entire architecture consists of user and control vertical planes as well as 3 horizontal layers, namely radio physical Layer (L1), radio link Layer (L2), and radio network Layer (L3) [8]. In control plane Layer 2 is further subdivided into Medium Access Control (MAC) protocol and Radio Link Control (RLC) protocol. In addition to MAC and RLC, the Layer 2 user plane contains 2 service-dependent protocols: the Packet Data Convergence Protocol (PDCP) and Broadcast/Multicast Control (BMC) protocol. In Layer 3, there is one Radio Resource Control (RRC) protocol in control plane.

The central idea of this layering protocol structure is to multiplex traffic flows of different kinds and origins. In layering system, a layer is created to encapsulate a collection of functions with similar objective. In context of UTRAN radio interface, it simplifies the design of service provision that varies in QoS requirement, coverage

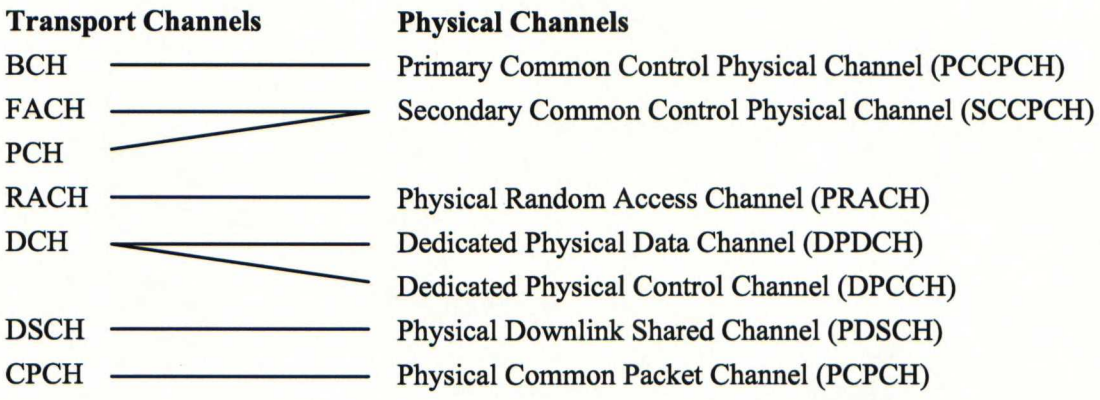

Figure 2.8: Transport channel to physical channel mapping

requirement, and rate requirement. It also conceals the details of layer implementation from other part of the system. Thus, continuing evolution of radio interface protocol such as HSPA can be carried out without affecting the entire architecture.

Physical layer provides its service to MAC layer via transport channels. It maps the transport channels to their corresponding physical channels as illustrated in Fig. 2.8. This mapping means that data and control signaling carried by transport channels are multiplexed into one or more physical channels with the restriction of physical radio frame formats. In this layer it directly carries out procedures that are essential for WCDMA system operation, including fast power control, paging, random access, cell searching etc [9].

The main responsibilities of MAC layer is to map logical channels to transport channels and multiplex data flows into transport blocks with dynamical scheduling and priority handling. This multiplexing is implemented with Transport Format Combination (TFC) selection from a TFC set (TFCS). At a given point of time, a TFCS defines all possible TFCs of multiple data flows carried by one or more transport channels, which will be encoded and multiplexed into a Coded Composite Transport Channel (CCTrCh). And it allows the resulting CCTrCh to change its individual data flow in data rate, including zero rate, and delay restriction on the basis of Transmit Time Interval (TTI) [10], which makes it possible to dynamically schedule user data.

RLC is mainly responsible for segmentation, retransmission and buffering user and control data. For each RB service, a RLC instance together with its buffer are

created [11]. The data from upper layer Protocol Data Unit (PDU) is segmented and put into RLC payload units in buffer. There are three operation modes of each RLC instance: transparent mode (TM), unacknowledged mode (UM), and acknowledged mode (AM). For all RLC modes, the Cyclic Redundancy Check (CRC) is added in the header of RLC PDU and checked in physical layer. In addition, AM uses an ARQ mechanism for error correction and retransmission is made in SRNC in case of erroneous reception. In control plane, RLC provides signaling RB services to RRC entity. In user plane, RLC provides RB services to upper layer if PDCP and BMC are not used, otherwise RB service is provided by PDCP or BMC.

The RRC protocol handles control plane signaling of Layer 3 between UE and UTRAN, as described in [12]. It interfaces to all the other protocols in Layer 1 and 2 to establish, configure and release connection between peer entities. The control signaling issued from higher layer is also encapsulated and transmitted in the RRC message payload, including mobility management, connection management, and session management.

2.5 HSPA evolution and LTE

User data rate and network latency are key aspects to define radio network performance and to enable radio services. In WCDMA the peak data rate has achieved up to 384kbps with 100-200ms latency. Yet, HSPA evolution process including HSDPA and HSUPA further boosts the data rate to 1-2Mbps in practice and beyond 10Mbps peak data rate with less than 100ms latency.

HSPA attains high data throughput by implementing new features including: fast physical layer retransmission, fast link adaptation and scheduling in HSDPA and fast base station scheduling in HSUPA [13]. These procedures are carried out in the radio interface by introducing new protocol entities in user plane as shown in Fig. 2.9. Compared with Fig. 2.7, the physical layer of terminals and NodeB are modified to support physical retransmission functionality. New entity MAC-hs located in NodeB is responsible for HSDPA base station scheduling and priority handling. The RNC still retains MAC-d entity, however, with transport channel switching functionality only. In HSUPA, base station scheduling is carried out by

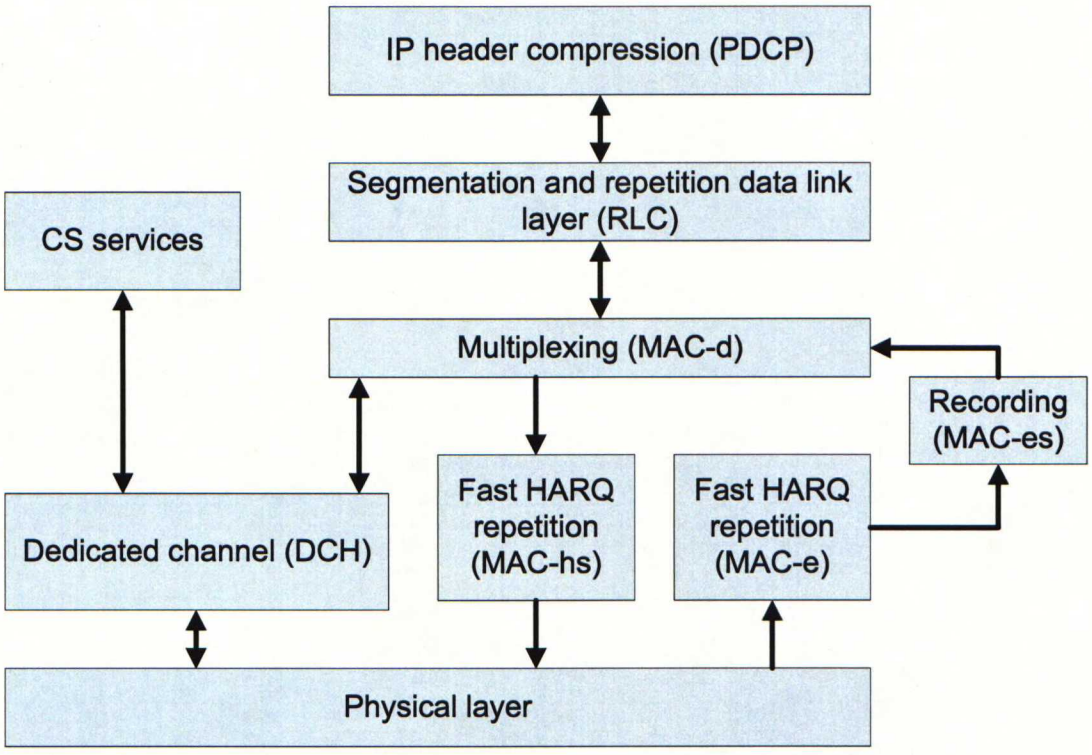

Figure 2.9: HSPA radio interface architecture for user data

MAC-e located in NodeB, while it is requested by terminal and controlled by RNC. Soft handover and macrodiversity combining are supported by HSUPA and they are carried out by MAC-es in RNC.

Table 2.3 compares the features supported by transport channels DCH (WCDMA), HS-DSCH (HSDPA), and E-DCH (HSUPA).

The newly introduced High-Speed Downlink-Shared Channel (HS-DSCH) carries

Table 2.3: Comparison of fundamental properties of DCH, HSDPA and HSUPA

	DCH	HSDPA(HS-DSCH)	HSUPA(E-DCH)
Variable SF	Yes	No	Yes
Soft handover	Yes	No	Yes
Fast power control	Yes	No	Yes
AMC	No	Yes	No
Multi-code operation	Yes	Yes, extended	Yes, extended
Fast L1 HARQ	No	Yes	Yes
BTS based scheduling	No	Yes	Yes

user data with HSDPA operation. It does not support variable SF and fast power control which are 2 fundamental features designed for WCDMA. In stead, the channel variation in downlink is utilized by fast link adaptation and scheduling to achieve so-called multiuser diversity gain. This means that the NodeB scheduler tends to allocates radio capacity to the UE with good channel quality in each HS-DSCH TTI. The communication path in good channel conditions allow to use a weak coding and high order modulation scheme and a large number of parallel codes, which enable a high data rate transmission. For better utilization of channel dynamics, 16QAM is added besides QPSK and up to 15 multi-codes can be used in parallel. In Release 7 HSPA+ the data rate is increased further by adding 64QAM, MIMO (Multiple-Input-Multiple-Output) and dual carrier operation.

The fast physical layer retransmission mechanism known as hybrid ARQ (HARQ) is also carried out in NodeB while RLC retransmission still exists in case maximum number of HARQ retransmission exceeds. In Layer 1 HARQ retransmissions are carried out and the data packets from all the retransmissions are stored in soft memory and combined before decoding procedure. The retransmitted packet can be either identical with the previous packet or in the form of incremental redundancy.

The Enhanced Dedicate Channel (E-DCH) introduced in HSUPA brings the similar features as HS-DSCH does in HSDPA, such as extensive multi-code operation and physical layer retransmission. Yet, unlike HS-DSCH, E-DCH is a dedicate transport channel and it does not allow fast scheduling based on instantaneous channel quality, because HSUPA scheduler is located in receiver side. Thus, the E-DCH scheduling is carried out based on estimation of instantaneous overall load level and it tries to maintain the interference that is proportional with the system load level as close to the maximum as possible. If the overall load level is estimated to exceed the allowed load level when a new session sets up, the scheduler will admit the new session while lowering the capacity allocated to old sessions.

The Long Term Evolution (LTE) was defined in 3GPP Release 8 with small enhancement in Release 9. It is introduced with a new wideband radio interface toward 4G system and has higher spectral efficiency compared with current technologies. Deployed over a bandwidth of 20MHz, Orthogonal Frequency Division Multiple Access (OFDMA) is used in downlink, which provides robustness against multipath inter-

ference and affinity to advanced techniques such as frequency domain scheduling and MIMO techniques. With a 4×4 antenna configuration, a peak data rate over 300Mbps is attained in downlink. In uplink Single-Carrier FDMA (SC-FDMA) is used to provide a high data rate with reduced power consumption. LTE provides a packet-only domain and it is optimized to IP services.

Together with the radio access technology evolution, a new network architecture evolution is also defined and denoted as System Architecture Evolution (SAE) in 3GPP specification. The SAE is proposed with a simplified flat network structure where the only element in radio access domain–eNodeB integrates all the functionalities carried out in the previous UTRAN into a single logical element, which both enhances the network throughput and reduces the traffic latency.

Chapter 3

Femtocell concept

3.1 Femtocell overview

In communication networks, the cellular concept is designed to reuse the same radio resources (time slot, frequency band or code) in different spatial area to extend the radio coverage throughout the target service area. The traditional cellular networks including UMTS are based on macro- or microcellular topologies and the radio access points - base stations aim to provide access service to users within an area from a few hundred square meters to square kilometers. The macrocell concept was initially designed to cater the low data rate service demand such as voice service and short message service and it is proved to be successful by commercial networks, such as GSM and UMTS.

From 2002, as the demand for high data rate service increases, 3GPP released its wireless broadband solution HSPA as a natural evolution of UTRAN. Although HSPA claims to have peak data rate 42Mbps in downlink and 5.76Mbps in uplink, the broadband property can be only held within a restricted area and cannot fulfill high rate that service needs throughout the network for several reasons. First, CDMA systems have so-called cell breathing effect and the coverage area of cell varies with its bearing load in wireless channel. Because of non-orthogonality among parallel transmissions in WCDMA as depicted in (2.7), the end receiver sees the signals from other transmission sources as interference to the desired signal. The interference acts as white Gaussian noise due to large number of users within the system and raises the effective noise floor at the receiver. With a limited transmission power,

the service coverage area will shrink to maintain the required signal-to-noise ratio (SNR) when cell load increases. Second, the request for high data rate connection causes a reduction in energy per bit level, which again causes required SNR level to be maintained in a restricted area around NodeB, service area being relatively much smaller than that under voice service. Third, radio propagation in 2GHz spectral band is vulnerable to non-line-of-sight condition. As a result, in a densely populated area, the user at cell edge or around large shadows, for example behind a wall, cannot obtain high data rates reliably.

Previous studies have shown that half of voice calls and a majority of data traffic originate from indoors. Thus, indoor femtocells cater these connection demands and create high-throughput hotspots overlaid onto macrocellular networks. In addition, the user-deployed femtocells aim to establish a win-win business model for both mobile operators and their subscribers, which provide the broadband wireless services to subscribers at a low price without putting too much burden on infrastructure budget of operators. As the femtocell equipment is acquired and deployed by users in their own family, there is a huge reduction in operators' OPEX and CAPEX investment, which includes budget spent on equipments and installation, monthly site lease and additional cost for electricity and traffic backhaul [2]. Thus, the femtocell deployment plan will economically expand the service coverage area along with the amount of service subscribers and make the operator to focus on provision of broadband services.

3.2 Status of standardization in 3GPP

The newly introduced femtocell concept also brings about the studies on femtocell architecture, to be exact, how the residence backhaul links are integrated into mobile operator's core network [14]. In May 2008 the discussions reached a consensus in Femto Forum and it lead to a joint Iuh interface proposal to 3GPP. As depicted in Fig. 3.1, a high-level view of the femtocell access network architecture includes 3 new logical elements: 3G Home NodeB, Home NodeB Gateway (HNB-GW) and Security Gateway (SeGW) [15]. Compared with UMTS network architecture in Fig. 2.4, these additional elements form a sub-network and make only minor changes

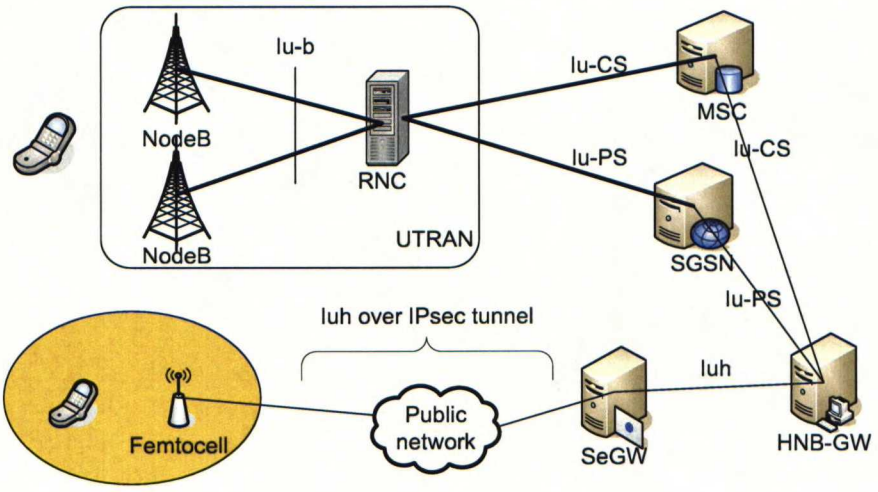

Figure 3.1: Femtocell architecture

to legacy network architecture.

The 3G HNB connects with mobile devices through the existing Uu interface. The interface standard is essentially kept unchanged, except for some minor modifications to employ femtocell specific features, such as CSG operation mode.

The HNB joins mobile operator's network through HNB-GW. The HNB-GW concentrates connections from a large amount of femtocells. This interface is defined in Release 8 as a new open interface Iuh and is responsible to transport user data and control signaling between HNB and HNB-GW. In addition, the Iuh connection is tunneled through public Internet by IPsec protocol and is secured by SeGW. SeGW acts as a firewall between operator core network and public Internet. It is located at operator premises and its physical implementation can be either as a separate device or as an integration with HNB-GW.

Connections from HNB-GW utilizes existing Iu-CS and Iu-PS interfaces to MSC and SGSN. HNB-GW acts as a large concentrator with a large number of HNBs and it is logically a standard RNC with a single Iu interface to the CN. From the perspective of CN, this satisfies the requirement of 3GPP system operator and device vendor that the inclusion of femtocell architecture does not affect the existing CN systems.

In the radio interface aspect, the potential radio interference introduced by femtocell has been concerned in the standardization process. It is unique due to the femtocell operating characteristics, deployment environment, management methods,

and security aspect. Considerable amount of investigations have been carried out by 3GPP RAN4 TSG to study robust and effective solutions that prevent excessive interference between femtocells, and between femtocell and existing macrocell networks [16]. In addition, the femtocell minimum performance specification that controls radio signal quality and interference aspects of devices is created to conform the UMTS radio standard community that femtocells can operate in a licensed spectrum. The specifications were originally created for macrocellular network deployment and thus, do not satisfy the needs of small, low-power, stand-alone femtocells that are deployed by users in uncontrolled environments. Thus, the minimum performance specification has been modified to take into account femtocell-specific issues such as timing accuracy requirements, transmission power classes and out-of-band emission requirements.

In security aspect, 3GPP was not able to reach a complete standardization in Release 8, yet a basic femtocell security architecture is agreed on and addressed in [17]. The mutual authentication of HNB and HNB-GW is carried out based on IKEv2 protocols that is defined in Internet Engineering Task Force (IETF). Encryption over the IP transport network between HNB and HNB-GW is performed using IETF IPsec protocols. The complete security standardization will be finished in Release 9.

The current standardization admits handovers only from femtocell devices to the macrocellular system, also referred as *hand-out*. Due to technical challenges and current development priority, handover from macrocell to the femtocell, referred as *hand-in*, is excluded from Release 8. Nonetheless, it is anticipated to have an open, interoperable ways to support hand-in in the next phase of standardization.

3.3 Technical motivation

Compared with traditional macrocellular topology, the femtocell concept is designed to distribute a massive number of smaller cells and locally carry out the radio traffic in reduced connection distance. This micro-ization process of cellular networks has been reflected in the evolution of radio communication history and is proved to be the main contributor in radio capacity improvement. It enables the cellular systems to

exploit a higher frequency band in the cell coverage area and allows to accommodate more user connections simultaneously. This huge capacity gain comes from the fact that smaller cells enable a higher spatial reuse of spectrum, which is equivalent of a higher area spectral efficiency [18].

Link capacity is defined as the information rate that can be transmitted over a given bandwidth and in AWGN channel it is given by Shannon capacity formula

$$\eta_e = BW \log_{10}(1 + SNR) \tag{3.1}$$

where BW is the operating bandwidth of the system and SNR is the link signal-to-noise ratio. In WCDMA system, SINR is given by (2.7), where the received signal power P_{RX}^d is a function of terminal transmission power, path losses, shadowing and transmitting and receiving antenna gains during the radio propagation. The transmission signal strength decays according to a distance dependent path loss $Ar^{-\alpha}$, where A is a constant path loss, r is the separation distance and α is the path loss exponent.

Therefore, the key to increase the link capacity of the channel between intended transceivers pair is to minimize r and the interferences from other transmissions. As indicated by this principle, the femtocell deployment has a higher area spectral efficiency than that of macrocell for several reasons. First, the range of femtocell is usually restricted to 10-20 meters. While signal reception is enhanced by shortening the separation distance between transmitter and receiver, the transmit power can be reduced. According to [2], the average transmit power saving by using femtocell can be as large as 77dB in comparison with that uses macrocell only. On the other side, the interference level from intra- and intercell decreases due to this power reduction, which further increases link SINR. Second, in macrocell operations the wall penetration leads to loss on desired signal, but in femtocells the penetration loss due to building walls becomes beneficial for femtocell deployment in case of proper installation. The walls well separate the spatial dominance of femtocell coverages and avoid excess interference in a dense deployments. Third, as the access to femtocell is mainly restricted within 1-10 subscribers, each user can be assigned with a larger portion of radio capacity. In HSPA, more code resources and scheduling slots can be allocated to one user if the total number of users being served is small.

3.4 Implementation challenges

In addition to the benefits femtocell brings, it is also found that challenges are arisen due to the introduction of new network structure. To lower the expenses of femtocell deployment, the base station installation is expected to be done by device owners themselves. Thus, operators are not able to configure the femtocells layout or even do not know their exact locations. By this uncontrolled nature, the femtocell and its underlaying macrocell will create mutual interference. It is especially heavy in CSG femtocell since only privileged users are entitled the access and interference from nearby macrocell users with strong transmission power cannot be alleviated by handover. Due to the loss of central management, the traditional methods for cellular network planning are not applicable any more and the interference between cells cannot be reduced by delicate site plan. In case of inappropriate installation, the femtocells with co-channel operation can severely deteriorate network performance [19].

In addition, it is practical to assume the users do not possess expert knowledge in setting up the femtocell. Only simple instructions are given as installation guidance, which should be a plug-and-play procedure similar with a WLAN access point set-up. Thus, the performability of a femtocell is much dependent upon its self-establishment and auto-configuration. After installation, femtocell is required to automatically adapt to the radio environment and set its operating parameters through negotiating with the network. However, the femtocell is also required to constantly adjust its transmission power since the surrounding environment is changed all the time.

The transmission of femtocell relies on the broadband backhaul capability in user premises. However, it is still in question to provide requested QoS for delay sensitive applications through femtocells as no delay resiliency is provided in current IP backhaul networks [2]. There is no guaranteed maximum level of delay and jitter in the network from broadband provider. Compared with dedicate backhaul in macrocell networks, it is even more difficult to backhaul the data through a shared transmission medium when other broadband transmissions occur, e.g. the broadband is simultaneously used by a computer.

The acquisition of a femtocell's location is another challenge to overcome though

it has important meaning in the context of a emergency call. In macrocell the network is able to track the position during an emergency call by measuring the distances between mobile phone and its neighboring base stations. Yet, as the position of femtocell is not aware of by operator, this method cannot be applied in a femtocell originated phone call. Although an additional GPS module equipped with femtocell might help in positioning, it is often problematic due to indoor installation of femtocell.

In this thesis we will concentrate our focus on the interference analysis of the femtocell systems and explore the possible method to suppress interference, because it is the most important challenge in the access stratum and draws most attention in the previous studies. The interference scenarios have been listed in [20] and preliminary 3GPP studies in different cases are summarized. These scenarios can be categorized into intra-tier interference which occurs between femtocells and cross-tier interference which occurs between femtocell and macrocell.

The intra-tier interference between femtocells includes FUE uplink interference to neighbor femtocell receiver and femtocell downlink interference to other FUE reception. In practical system, it is more reasonable to deploy femtocells in a single band due to scarce spectrum resource. However, as the user density increases, sever interference may occur between neighboring femtocells if their dominant regions are sufficiently close to each other. Such situation is likely to happen when femtocells are deployed in a MDU where multiple apartments are placed close to each other and direct path between two neighbor femtocells is short on average. The signal can easily leak to other cells due to lack of radio isolation. The femtocell radio performance is sensitive to the deployment layout, especially under CSG mode. Fig. 3.2 depicts a worst case when two femtocells are improper installed within two neighbor apartments, which are separated by a single wall (midmost horizontal wall in Fig. 3.2). Both of the user terminals are located near their interfering femtocells, while far from their serving nodes. If the apartments are not well separated, e.g. the separating wall is not a load-bearing wall and interference from other cell can penetrate into own cell with a relatively strong level, the uplink power control mechanism in both UEs will increase their transmission powers at the same time, which results in uplink power competition. Similarly, the downlink transmission in the same configuration

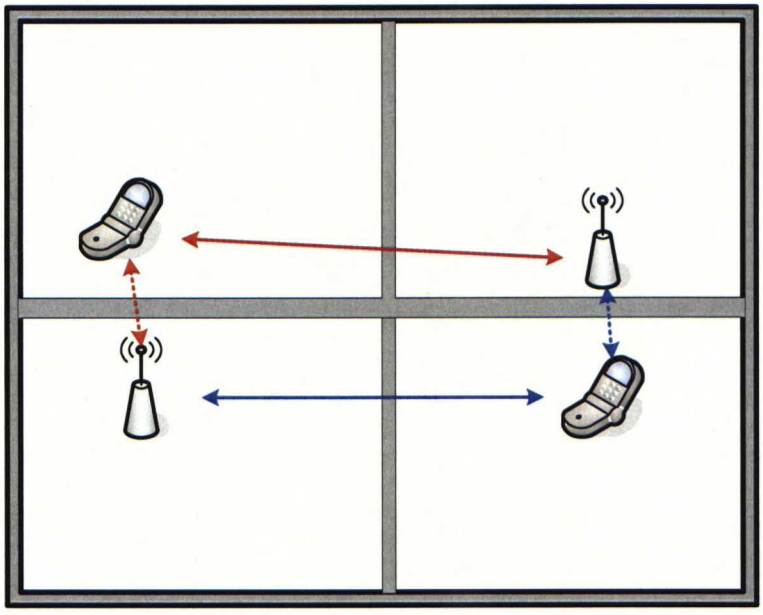

Figure 3.2: Femtocell intra-tier interference

also suffers a dominant interference level from adjacent cell due to the absence of handover between CSG femtocells. In these scenarios, [19] proposed an interference avoidance method in uplink channel, which jointly utilizes a flexible spectrum usage scheme and femtocell beamforming. In addition [21] compares the analytical results by incorporating a downlink interference suppression method among femtocells.

Due to the unorganized nature of femtocells, they may disturb the performance of existing macrocell networks that are deployed by central planning, or vice versa. So it becomes an important research topic to suppress the performance degradation under the condition of femtocells' disorganization. The mutual interference occurs between macrocell and femtocell in both uplink and downlink as summarized in scenarios 1-4 of [20]. Our discussion is mainly focused on the co-channel operation, and assumes the receiver can well suppress adjacent channel interferences. The main interference scenarios are

1. **UL HNB UE to Macro.** This scenario happens when a MBS is close to an active FUE that transmits at the maximum power. Even worse, in line-of-sight condition, the transmission power from FUE will cause a high interference at MBS and increase noise rise to all serving UEs under this MBS. However, in the same situation, the femtocell pilot reception at FUE is also impaired

by downlink interference from MBS. Hence, the probability of this scenario is relatively small because femtocell coverage is limited to a short range and FUE transmission can rarely cause strong interference to MBS reception.

2. **DL HNB to Macro UE.** A fully loaded FBS is located inside a building where there is weak macrocell signal coverage. The transmission power of the femtocell will flood the nearby MUEs signal reception from MBS and create macrocell coverage hole.

3. **UL Macro UE to HNB.** A MUE is located indoor or at cell edge where macrocell signal coverage is weak. The uplink power control procedure will drive this MUE to transmit with its maximum power level and it would interfere the nearby femtocell receiver. Together with scenario 2, they are relevant only when CSG access is used and the MUE is not entitled the access to femtocell.

4. **DL Macro to HNB UE.** In this scenario, a fully loaded MBS with its maximum transmitting power is close to an active FUE that is located at the edge of its serving femtocell. However, in this case, the FUE would have a good macrocell service experience and leave femtocell unused. Some mechanism that encourage user to re-deploy the femtocell would be helpful.

In the previous studies, results have proved the deployment of femtocells with open access has only small effect on macrocell networks, which is minor compared with huge overall throughput improvement [22]. Holger Claussen et al. further proposed methods to optimize the femtocell coverage area by minimizing the macro- and femtocell mobility event in [23] and [24].

3.5 System model

To simulate the femtocell system, we need to present a system model that fit with the practical femtocell operation mode and operation environment. Due to the fact that the ownership of a HNB usually belongs to a family or household member, the usage of HNB is restricted within the room or apartment and handover between adjacent HNBs is not allowed. In contrast to macrocell deployment, HNBs are

independently installed by users themselves. The placement position of HNB and the building structure cannot be regulated, which leads to an uncoordinated HNB deployment scenario. In this section, we propose a MDUs building structure that serves as our indoor environment model. The rationale behind this selection is that they account for over half of all residential dwelling types in the country of study, Finland [25].

3.5.1 Uplink model

The indoor propagation model is the so-called Motley-Keenan model, where a wide-band single-tap signal at direct path dominates the reception. In the indoor environment, the radio propagation is also weakened by accumulated wall attenuation. Thus, the total indoor path loss is modeled as

$$PL_{indoor} = PL_D + PL_W + PL_F, \tag{3.2}$$

where PL_D is the distance dependent path loss, PL_F is a Rayleigh distributed fast fading that accounts for constructive and destructive addition of multipath components introduced by radio waves reflection, diffraction and scattering. And PL_W is the accumulated wall attenuation along the direct propagation path, which is calculated by

$$PL_W = N_{thick} \times L_{thick} + N_{thin} \times L_{thin} + N_{floor} \times L_{floor} + N_{win} \times L_{win} \tag{3.3}$$

where L_{thick} is the thick wall attenuation that is used when penetrating the outer wall of the building. The wall attenuation between rooms and/or separated apartments is denoted by L_{thin}. Notation L_{floor} is used for floor attenuation and L_{win} refers to window attenuation. N_x(x is *thick*, *thin*, *floor* or *win*) is the number of walls/floors/windows penetrated for each type.

In outdoor environment, the total path loss is given by

$$PL_{outdoor} = PL_D + PL_S + PL_F, \tag{3.4}$$

where PL_D is outdoor average path loss which can be calculated by empirical path loss model such as Okumura-Hata or Walfisch-Ikegami model. The PL_S denotes the shadow fading between MBS and MUE. Shown by measurement campaigns, shadow

fading fits a log-normal distribution well. After selecting a standard deviation σ_S, PL_S can be randomly generated as a Gaussian variable (in decibels).

As indicated by (2.7), the post-pocessing SINR $(E_b/N_0)_d$ at the FBS d is calculated by

$$(E_b/N_0)_{UL}^{FBS_d} = SF\frac{P_{RX}^{FUE_d}}{\sum_{i=1}^{N,i\neq d} P_{RX}^{FUE_i} + \sum_{j=1}^{K} P_{RX}^{MUE_j} + N_0} \tag{3.5}$$

where $P_{RX}^{FUE_d}$, $P_{RX}^{FUE_i}$ are received signal powers at FBS d from desired and interfered FUEs, $P_{RX}^{MUE_j}$ is the received signal power from MUE j. In terms of UE transmission power and path loss, values of these signal powers seen by FBS are calculated from

$$P_{RX}^{FUE_x} = \frac{P_{TX}^{FUE_x} \times G_A}{PL_{indoor}}, \qquad x \in \{i, d\} \tag{3.6}$$

$$P_{RX}^{MUE_x} = \frac{P_{TX}^{MUE_x} \times G_A}{PL_{outdoor}}, \tag{3.7}$$

where G_A is compound antenna gain contributed by antennas of both transmitter and receiver.

Due to the near-far effect in WCDMA radio interface, power control is needed so that according to certain service requirement, a target received $(E_b/N_0)_{UL}$ ratio is fulfilled. However, in case target $(E_b/N_0)_{UL}$ is not attained when the power control hit the maximum value, an outage event happens and the FUE is marked to be in *outage*.

3.5.2 Downlink model

In downlink direction, the received $(E_b/N_0)_{DL}$ ratio is also calculated with (3.2)–(3.4) but with constant transmission power $P_{TX}^{FBS_x}$ or $P_{TX}^{MBS_x}$. Thus, (3.5)–(3.7) are rewritten for downlink channel as follows

$$(E_b/N_0)_{DL}^{FUE_d} = SF\frac{P_{RX}^{FBS_d}}{\sum_{i=1}^{N,i\neq d} P_{RX}^{FBS_i} + \sum_{j=1}^{K} P_{RX}^{MBS_j} + N_0} \tag{3.8}$$

$$P_{RX}^{FBS_x} = \frac{P_{TX}^{FBS_x} \times G_A}{PL_{indoor}}, \qquad x \in \{i, d\} \tag{3.9}$$

$$P_{RX}^{MBS_x} = \frac{P_{TX}^{MBS_x} \times G_A}{PL_{outdoor}} \tag{3.10}$$

3.6 Special application of femtocells: public safety framework

Previous study has shown the importance of prehospital care in the resulting patient's survival [26]. The patient with serious injuries of head, spinal cord and internal organs requires to receive dedicate care at the emergency site and during the transportation. Such prehospital care is crucial for the future of the patient. Yet, emergency medical paramedics, who are the first professional personnel handle the patient, are able to provide general prehospital medical care do not required to have specific knowledge to deal with the situation. Due to financial and practical restriction, it is not possible to routinely deploy specific experts in onsite EMPs team, such as neurosurgeons, cardiologists, orthopedics, etc. However, onsite EMPs can rely on the directions from remote experts, provided the sufficient information and status of the patient are available to the experts.

Prehospital telemedicine is known as delivery of health care and sharing of medical knowledge through telecommunication systems from a remote site before patient's hospitalization. It aims to virtually "bring" the expert surgeons to emergency site by means of high-resolution medical scan image transfer, high-volume biosignal data telemetry, streaming video, videoconferencing, location-based services and other rich multimedia services. Thus, remote surgeons can provide professional consultation to onsite paramedics and take part in decision-making processes regarding need for specific procedures, further diagnostics and hospital of destination.

In order to meet the data rate required by the aforementioned services, it is would be practically and economically feasible to carry out services provision based on existing broadband mobile networks. It is natural evolution from early emergency telemedicine system that employed conversational voice and low bit-rate data telemetry through mobile radio between emergency site and receiving hospital or trauma center and emergency dispatch center [27].

3.6.1 Communications infrastructures

Several candidate wireless networking technologies are considered for providing multimedia emergency telemedicine services, yet, their implementations are limited by

intrinsic limitations. The authority-owned professional mobile radio (PMR) networks (usually standardized by Terrestrial Trunked RAdio or TETRA) are designed for dedicated use by emergency response organization in the situation of disasters, fire, flood or other mission-critical operations [28]. The terminal under TETRA Release 1 (R1) operates in a licensed spectrum from 380MHz–400MHz, thus, possesses security, robustness and service prioritization in the radio traffic exchange. Moreover, TETRA standard admits an ad-hoc operation mode – direct mode and allows mobile nodes communicate without a fixed base station. It is especially meaningful in the context of large-scale disaster when terrestrial infrastructure is destroyed or lacking in base station radio coverage. However, the maximum data rate defined in TETRA Release 1 is not comparable with commercial systems and can only fulfill the demand for voice, low-speed data service and slow-scan video services. The subsequent TETRA Release 2 standards, also referred to as TETRA Enhanced Data Services (TEDS), is upgraded with an enhanced air interface standard and supports a peak data rate up to 500kbps [29]. But the implementation of TEDS is still restricted due to lack of a internationally suitable harmonized spectrum band, which also results in a situation that very rare devices are upgraded to TEDS standard in the market.

Therefore, it is natural for emergency response organizations to utilize commercial public 2.5G or 3G mobile networks to provide services that require higher data rate than that TETRA Release 1 can achieve [30]. The continued evolution beyond 3G (e.g. HSPA) further increases the achievable data rate significantly above 384kbps, which easily exceeds TEDS data rates. This trend is also backed by the increased availability of dual-mode devices that are equipped with both TETRA and non-TETRA interfaces. By means of auto-sensing and auto-selection, the devices take advantage of benefits from both of PMR and commercial networks. However, due to lack of exclusive use priority, the emergency telemedicine services carried out through public networks may be degraded by an unpredictable throughput and delay fluctuation due to changes in macrocellular traffic or load pattern. Furthermore, achievable performance of 3G network would be further degraded by poor indoor coverage or geographic obstacles as stated in previous chapter.

This chapter proposes a use case scenario of emergency telemedicine service delivery

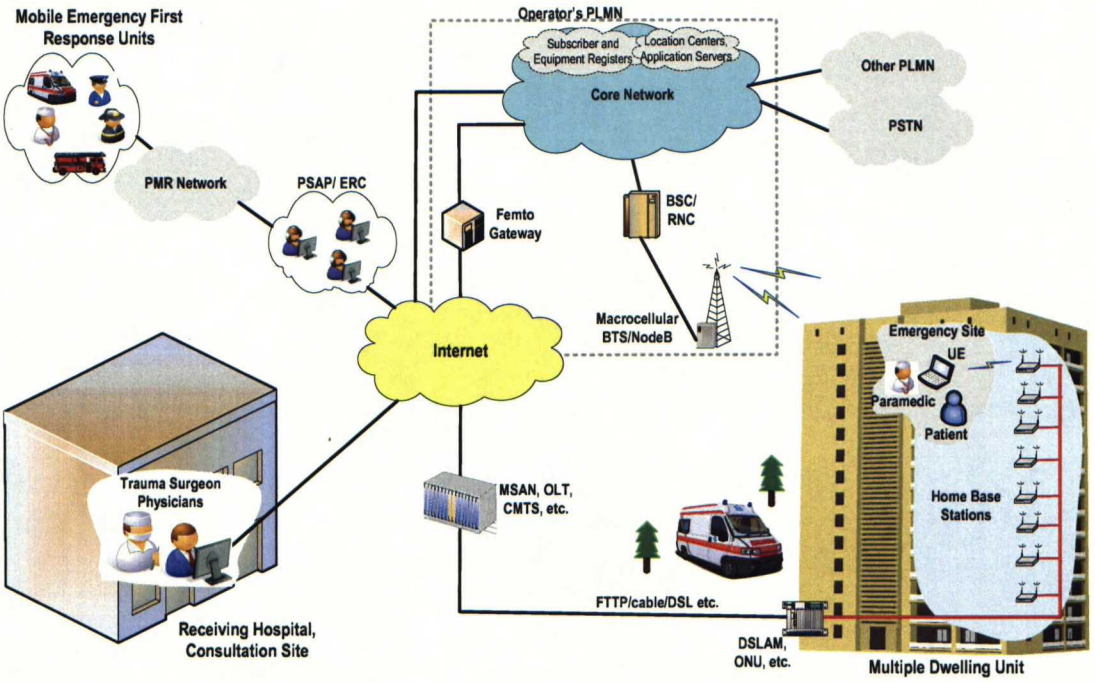

Figure 3.3: General system architecture

based on 3G femtocellular networks. From perspective of this service implementations, the femtocellualr approach inherits all benefits of service provision based on commercial networks. It is further improved with a better indoor coverage in comparison with purely macrocellular implementation [2]. Moreover, the UE involved to carry out videoconferencing and transmission of medical telemetry would have a prolonged battery life and at least an order of magnitude improvement in capacity gains. Due to access restriction set by CSG femtocell mode, a much smaller number of UEs is expected to be connected with the FBS, and the service QoS is guaranteed at a certain extent. The end-to-end system architecture illustrating the key network components and main actors in the femtocellular emergency telemedicine system is shown in Fig. 3.3.

3.6.2 Study Case Description and Assumptions

Fig. 3.4 depicts the complete use case scenario description for our study. This section proposes the usage of indoor femtocellular network to provide emergency

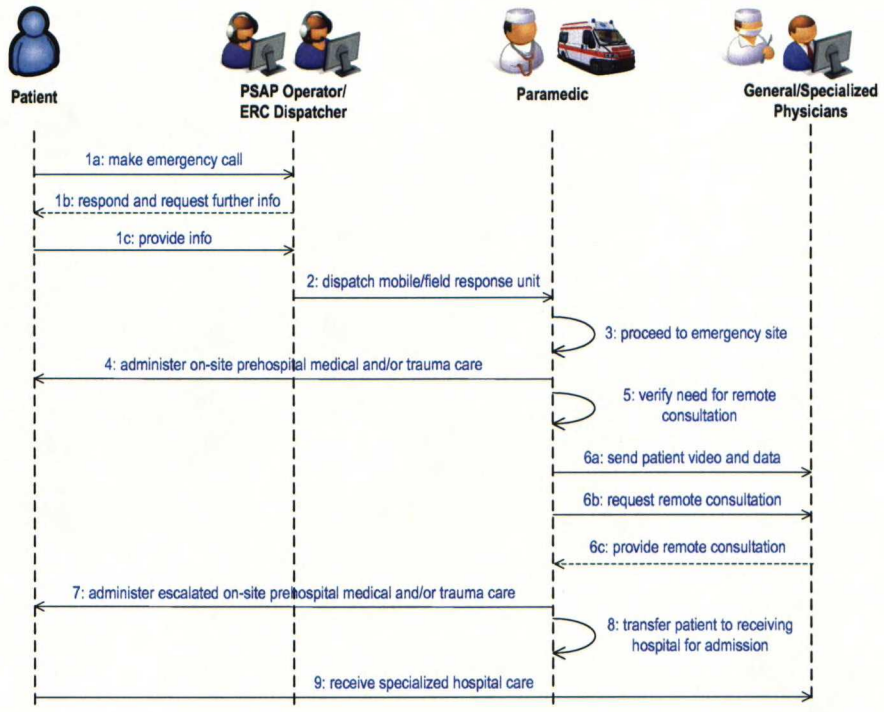

Figure 3.4: Use case description sequence diagram

telemedicine service shown as 6a-6c in Fig. 3.4. It is performed at the initial location of emergency and prior to patient transfer via ambulance. By means of simultaneous videoconferencing, telemetric biosignal transmission and medical image scans, it would allow surgical experts at remote hospital to virtually take part in the emergency treatment and decision-making processes. The service QoS parameters

Table 3.1: Emergency telemedicine service QoS requirement in UMTS network

Medium	**Application**	**Degree of symmetry**	**Data rate**	**Key performance parameters and target values.**		
				End-to-end one-way delay	Delay variation within a call	Information loss
Video	Videophone	Two-way	32-384 kbps	< 150 msec prefered; < 400 msec msec limit		< 1% FER
				Start-up delay	Transport delay variation	Packet loss at session layer
Data	Still image	Primarily one-way		< 10 sec	N/A	Zero
Data	Bulk data transfer	Primarily one-way	< 384 kbps	< 10 sec	N/A	Zero

are aligned with 3GPP QoS class and summarized in Table 3.1 [31]. Trauma device platforms and software clients providing an environment for running simultaneous applications have been previously demonstrated in [30].

The emergency location of the patient considered in the study is an indoor residential environment of MDUs structured as homes or apartments in a mid/high-rise with each floor having multiple apartments. Furthermore, the simulation study is repeated for MDUs structured as terraced (horizontal) buildings with multi-floor apartments (typically two floors per apartment).

Chapter 4

Simulation results

System level simulations are carried out in order to analyze the interference impact in the femtocell use scenarios. The conclusions are made by gathering the statistical results of uplink outage rates and possible downlink throughputs. Moreover, based on femtocellular network infrastructure, the provision of emergency telemedicine application is verified by simulations.

Under the assumption of 3G femtocellular deployment with CSG operation, the interference sources seen by FBS/FUE can be categorized into 3 cases. First, there are the transmissions from other FUE/FBS in neighbor femtocells. If nearby femtocells are not well separated by walls, it might result in bad performance for both of the femtocells as shown in Fig. 3.2. Second, there is the interference transmission from MUE/MBS. In a co-channel deployment scenario, the capacity provided by femtocellular network may be badly degraded when there is a line-of-sight condition between MBS and FUE or when a nearby MUE is transmitting with a high power. Third, there are transmissions from other FUE/FBS. Table 4.1 summarizes the aforementioned interference scenarios together with the corresponding practical factors that may affect to the interference level.

For the interior structure of MDU-type building, the simulator applies a simplified building model to agree with the assumption, as depicted in Fig. 4.1. The inside apartments are placed on a regular grid and each apartment has the same room layout. Each apartment admit dimensions $10m \times 10m \times 4m$, and it is divided into 4 equal size rooms by two crossing walls. Each room is of size $5m \times 5m \times 4m$. A similar building model is proposed in 3GPP [32]. The FBS, denoted by red square in

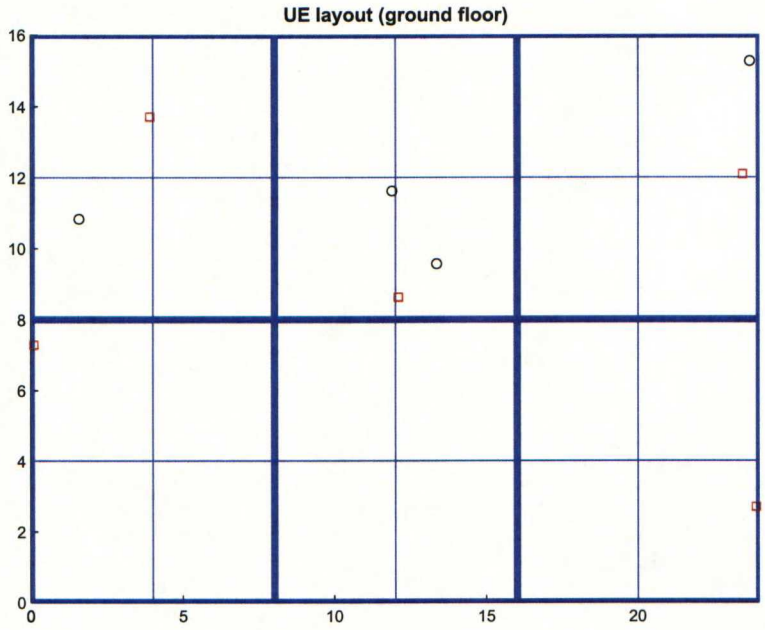

Figure 4.1: Example of a 3×2 grid floor layout

Fig. 4.1, is assumed to be deployed randomly on one of the walls in the apartment. FUEs are uniformly distributed in the apartment and shown as black circles.

The number of FBSs deployed in the building is determined by femtocell penetration rate P_{femto}. The connection between FUE and FBS pair is formed only when they are in the same apartment, otherwise the indoor UE is served by an MBS. Moreover, FUE is allowed to be handed over to MBS but not to another FUE.

The simulation results to be shown in the next sections are aimed to carry information on femtocell performance in a statistical sense. In uplink results are analyzed in

Table 4.1: Interference source

Interference source	Influence factor
Interference from other femtocell	Building structure Wall attenuation Spectrum usage scheme
Direct interference from macrocell	Apartment elevation Spectrum usage scheme Window attenuation
Indirect interference from macrocell	Window attenuation

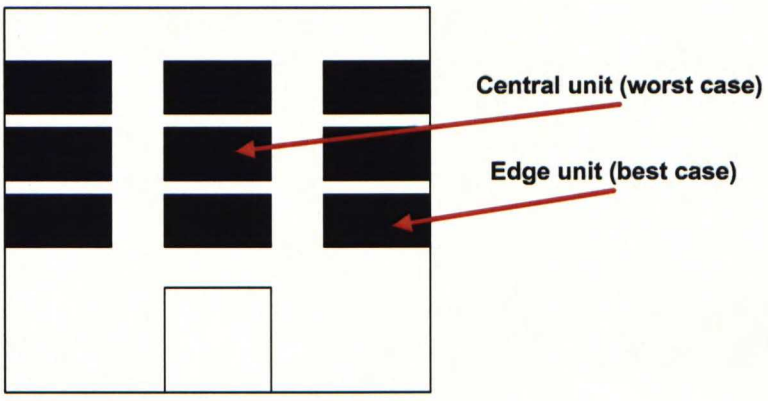

Figure 4.2: Apartment block

the form of Cumulative Distribution Functions (CDFs) of FUE transmission power. It is relevant method in that the uplink outage rate is revealed by the CDF where UE transmission power exceeds the maximum. In downlink the CDFs of channel spectral efficiency are calculated and illustrate how much channel capacity can be exploited by femtocellular deployment.

4.1 Notation and convention

Building dimensions. The block dimension is determined by the number of apartments in x, y and z axis (floor axis). We will denotes the block dimension as $B{:}m \times n \times p$, where m is the number of apartments in x axis, n is the number in y axis, and p is the number in z axis. The apartment's dimensions are given as the number of rooms within alongside x, y, and z axis, which is denoted as $A{:}m \times n \times p$. Each room is dimensioned by its length, width and height in meters, which are denoted as $R{:}m \times n \times p$.

Best and worst cases. Due to regular layout, we have a central apartment (shown in Fig. 4.2) in our interests, and it is referred as the worst case since it is fully surrounded by neighbors. Similarly, we are also interested in the apartment at the edge of the building block, which is referred to a best case since indoor interference source are limited by building structure.

Heavy and light wall. Usually, the walls separating rooms and apartments are different in thickness, which results in different penetration loss. In the follow-

Table 4.2: Femtocell framework simulation parameters

Mobile assumptions	
Maximum transmission power	21dBm
Antenna gain	0dBi
Base station assumptions	
Maximum transmission power	43dBm (MBS) 21dBm (HBS)
Null steering gain	6dB
Eb/N0 requirement	7dB (384kbps in uplink)
Path loss model	
Indoor	Keenan-Motley
Outdoor	Okumura-Hata
Carrier frequency	2GHz
Wall penetration loss	
Window loss	5dB
Building's outer wall and floor	15dB
Building's inner wall loss	8dB (thin wall) 15dB (thick wall)

ing discussion, we will assume the wall between rooms within a single apartment is fixed to be 8dB and penetration loss of the wall between 2 apartments can vary between 8dB (for light wall) and 15dB (for heavy wall). In addition, floor and building's outer wall are characterized by 15dB loss.

4.2 Femtocell downlink and uplink performance simulation

This section presents the simulation results regarding with femtocell performance in both uplink and downlink. Femtocells are assumed to be fully deployed in building, i.e. $P_{femto} = 1$. The simulation parameters are summarized in Table 4.2.

4.2.1 Effect of building dimensions

In uplink direction, we are interested in how the building block's dimension will effect on the femtocells' performance. The building's dimensions are ranged from $B : 3 \times 1 \times 3$, $B : 5 \times 1 \times 5$,..., to $B : 8 \times 1 \times 8$. Simulations have been carried

out for both light and heavy walls. Both of the simulations assume femtocells and macrocells operating in the same band. There is a single active FBS and FUE pair in each apartment. The CDF of transmission power of central apartment's FUE is shown in figures 4.3 and 4.4.

From the results, we see that the FUE's transmission power is pushed higher by power control procedure in light wall building and also the outage rate is higher than that in heavy wall building. However, in both cases, the outage rates are independent of the building's dimensions. The reason of this independence is that the main interference sources that cause outage are the transmissions in apartment's close neighbors. The interference from FUEs in other apartments is attenuated by at least 3 walls and the resulting power strength at reference femtocell is at least 15dB less than the one from main interferer, so that they cannot contribute much to the final outage rate.

We also have identified the fact that at low transmission power range, the 4 curves (B:$5 \times 1 \times 5$, B:$6 \times 1 \times 6$, B:$7 \times 1 \times 7$, B:$8 \times 1 \times 8$) in each figure are grouped with similar CDF and the curves in each group have the reference apartments from same floor level. Due to use of height dependent Okumura-Hata model, the apartments at the same floor level are under similar MUE interference. At low FUE's transmission power region, the curve is mainly affected by MUE interference as long as it is fully surrounded by neighbors. However, as transmission power increases, macrocell interference cannot be comparable with total receiving power. This height dependent effect fades and all the curves converge into same outage rate.

4.2.2 Dominant interference

In grid building structure with densely deployed femtocells, we are interested in the distribution of strongest interferer in the building and how the building walls can attenuate interference that comes from other femtocells. In the following uplink simulations, in each drop, we pick up the position of FUE that produces with greatest interference power with respect to the reference femtocell, so to generate the main interference distribution. Simulations are carried out under both the condition of light and heavy inner wall respectively, and both of the simulations assume a building of dimensions $B : 5 \times 5 \times 1$. No MUE interference is present.

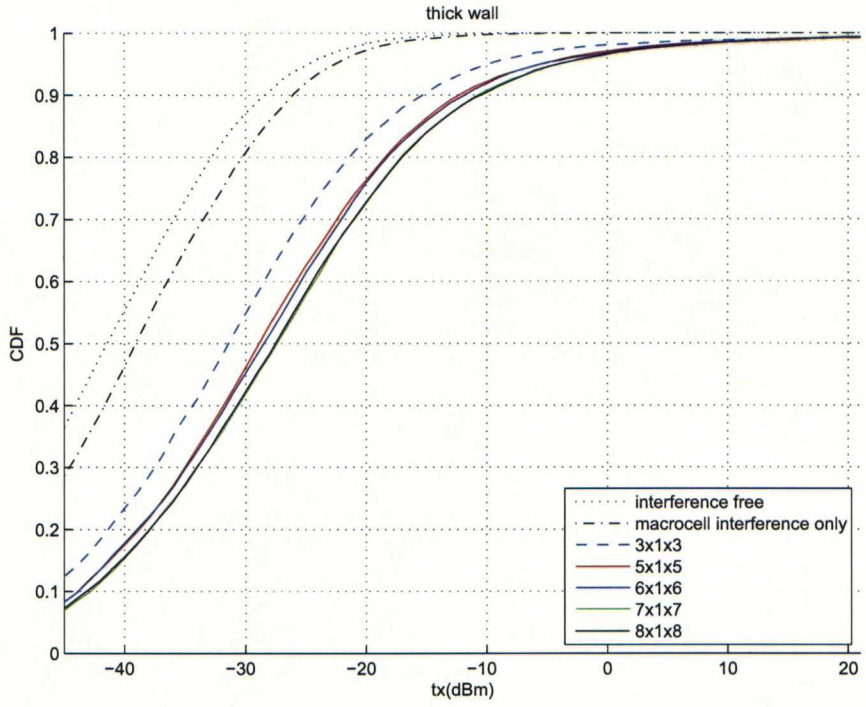

Figure 4.3: CDF of HUE's transmission power in a heavy wall building.

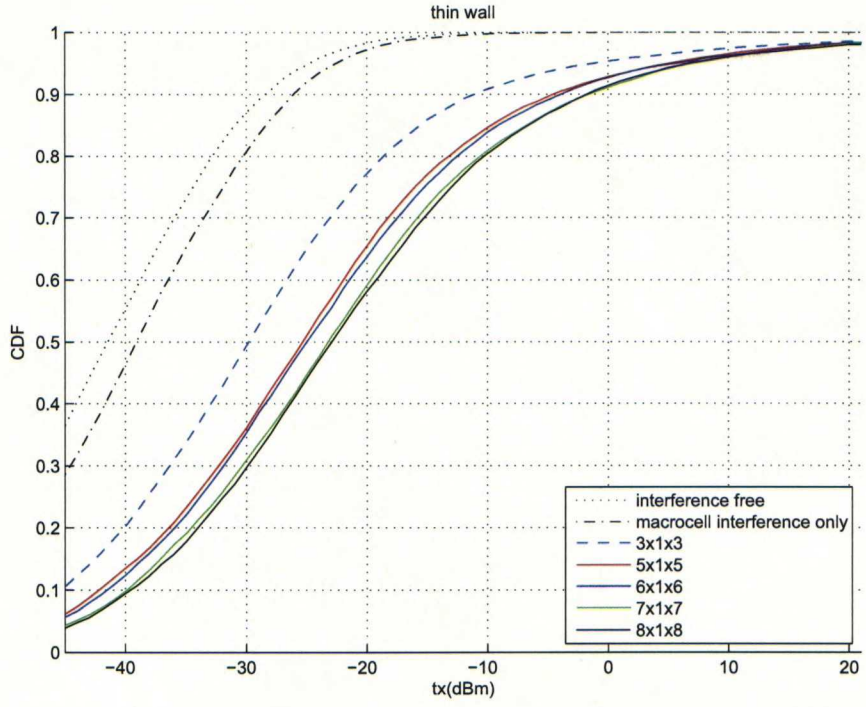

Figure 4.4: CDF of HUE's transmission power in a light wall building

Figures 4.5 and 4.6 show that in block of flat environment, interference from other femtocells mainly come from the neighborhood of our reference apartment, especially from the 4 closest neighbors because of less wall attenuation. The heavy wall (15dB penetration loss) structure even further reduce the interference effect from other apartments. This result is, again, a verification for our statement about irrelevance of building dimensions.

4.2.3 Effect of flexible spectrum usage

In the following discussion, we propose three different spectrum usage schemes that will be used.

(A) Both MBSs and FBSs operate in the same frequency band

(B) MBSs and FBSs operate in exclusive frequency bands

(C) FBSs use exclusive band but may switch to macrocell band as secondary users if interference situation becomes critical

Now we conduct the following simulations to compare uplink CDF of FUE's transmission power with different building dimensions and wall attenuations under these three schemes.

When deployed in an additional band, the FUE's average transmission power in reference apartment is lowered and CDF approaches interference free curve, especially at the low transmission range. But when FUE transmits with a higher power (more than 0dBm), this performance difference between schemes (A) and (B) decreases. Finally, the additional band surprisingly does not lower the femtocell's outage rate, because total receiving power from other femtocells, which cannot be reduced by this exclusive femtocell band, overwhelms MUE interference (with about 30dB difference).

However, because of dimension irrelevance, interference from apartments other than neighbors have only limited impact on the reference femtocell. So by forcing only few femtocells (at maximum 10% of total femtocells) to operate on another band, the interference can be efficiently reduced so that resulting CDF curve in femtocell band will approach the interference free case.

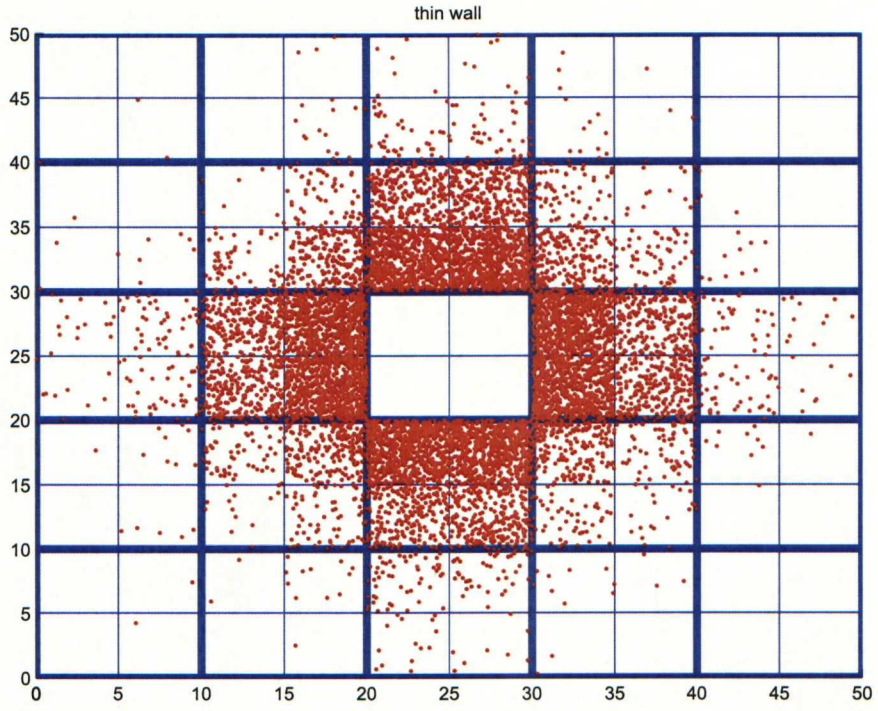

Figure 4.5: Distribution of dominant interference source in a light wall building

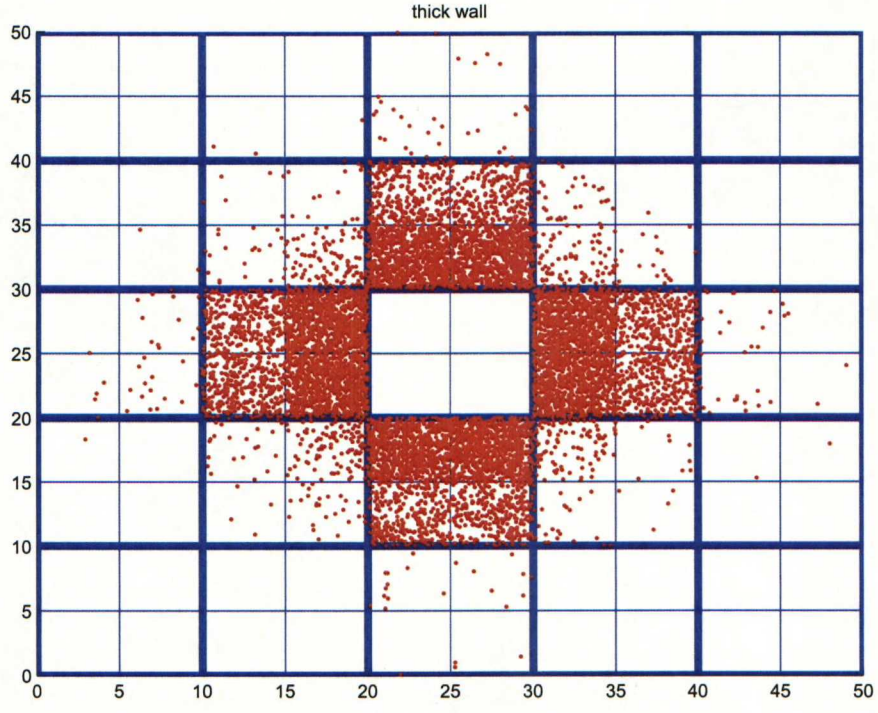

Figure 4.6: Distribution of dominant interference source in a heavy wall building

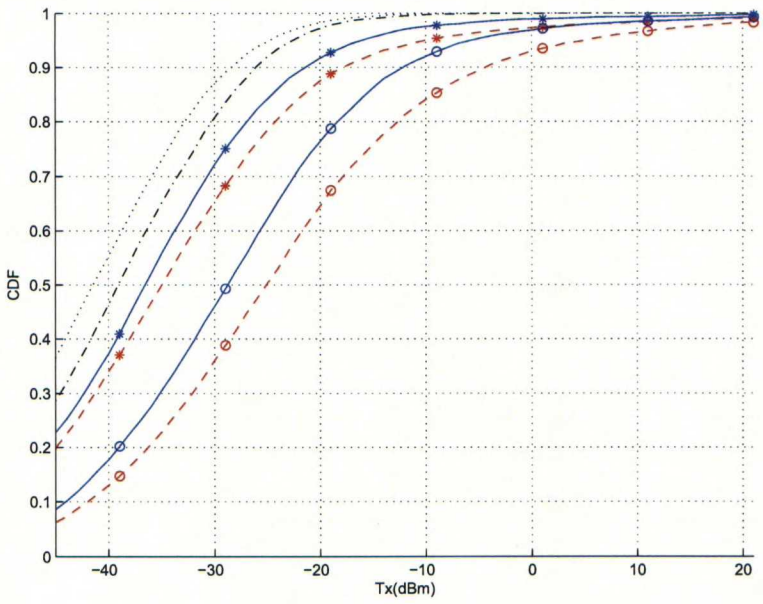

Figure 4.7: Femtocells under condition (A). Dotted curve: interference free, dashdot curve: MUE only, solid curve with star: B:$3 \times 1 \times 3$ with heavy wall, dashed curve with star: B:$3 \times 1 \times 3$ with light wall, solid curve with circle: B:$5 \times 1 \times 5$ with heavy wall, dashed curve with circle: B:$5 \times 1 \times 5$ with light wall.

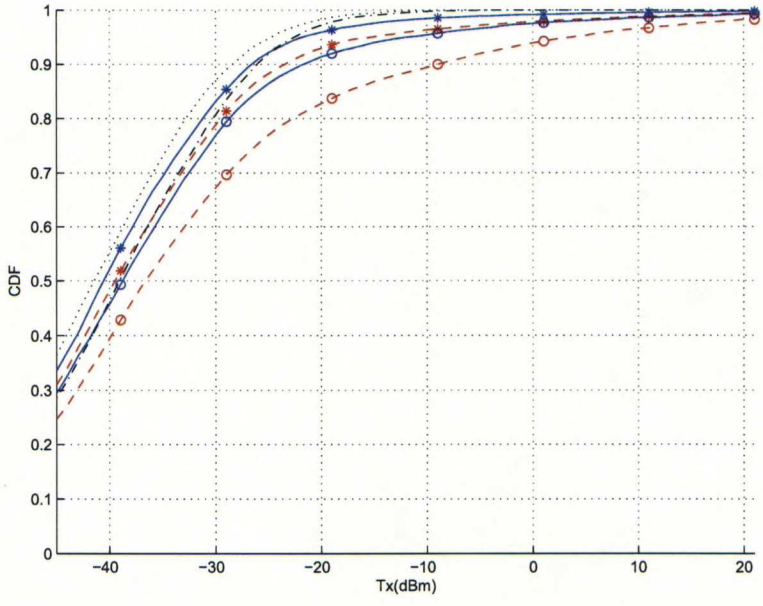

Figure 4.8: Femtocells under condition (B). Dotted curve: interference free, dashdot curve: MUE only, solid curve with star: B:$3 \times 1 \times 3$ with heavy wall, dashed curve with star: B:$3 \times 1 \times 3$ with light wall, solid curve with circle: B:$5 \times 1 \times 5$ with heavy wall, dashed curve with circle: B:$5 \times 1 \times 5$ with light wall.

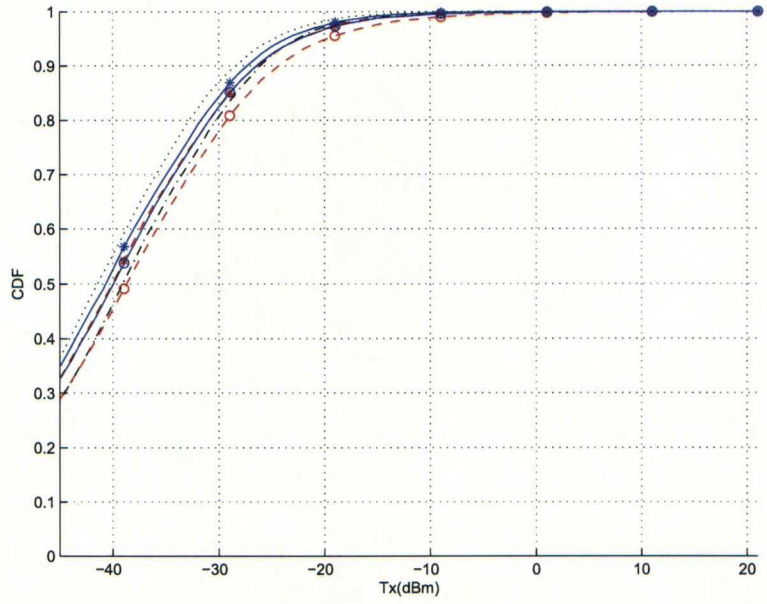

Figure 4.9: Femtocells under condition (C). Dotted curve: interference free, dashdot curve: MUE only, solid curve with star: B:$3 \times 1 \times 3$ with heavy wall, dashed curve with star: B:$3 \times 1 \times 3$ with light wall, solid curve with circle: B:$5 \times 1 \times 5$ with heavy wall, dashed curve with circle: B:$5 \times 1 \times 5$ with light wall.

4.2.4 Effect of Window Attenuation

The typical attenuation value for a window is 5dB. We aim to examine to what extent the window can raise the effect of MUE interference, and how the window position affects. The window effect is added to reference apartment, neighbor's apartment, and far-end apartment respectively. The dimensions of building are B:$5 \times 1 \times 5$, and femtocells and macrocell are operating in the same band.

When window is attached on the reference apartment, the portion of FUEs with low transmitting power (-45dBm to 0dBm), on which macrocell interference has main impact, is shrinking. But when window is attached on neighbor's or far-end apartment, the curves do not change much in comparison with no-window case. This shows the fact that indirect interference from macrocell does not affect to the reference femtocell a lot.

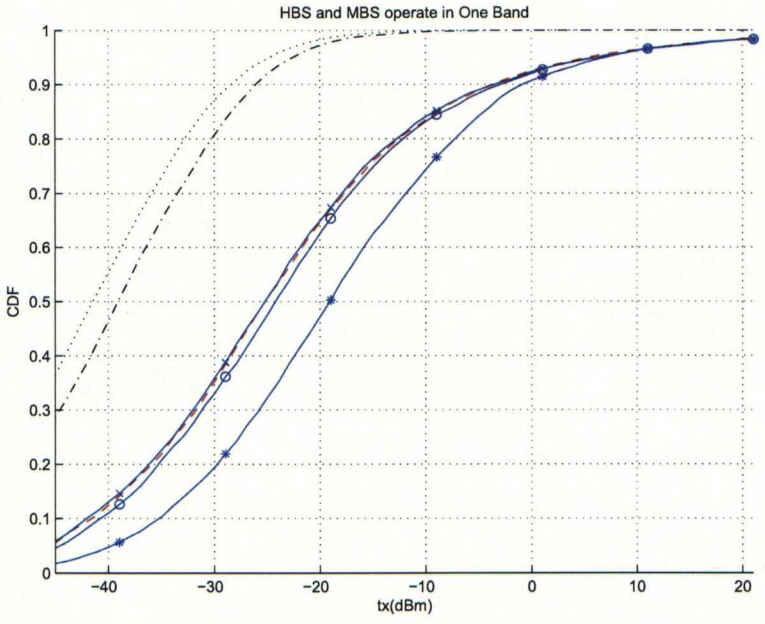

Figure 4.10: Window effect. Dotted curve: interference free, dashdot curve: MUE only, dashed curve: no signal through window, star curve: direct interference through window, circle curve: interference through window in neighbor, × curve: interference through window in far-end apartment

4.2.5 Downlink spectral efficiency

To avoid complicated assumptions about underlying system, spectral efficiency is calculated by (3.1).

Simulations are carried out in the building with dimensions B:3×1×3 and B:5×1×5. Heavy and light wall between apartments are examined respectively. The result are collected from both central apartment and edge apartment.

From Fig. 4.12, where MBS interference is not present, it is found that the downlink spectral efficiency of FBS is not influenced largely by building's dimensions, but rather by penetration loss of walls and the FBS's position in building, which is a prove for dimension irrelevance in downlink direction. However, in Fig. 4.11, the spectral efficiency curves of central apartments are grouped due to heavy MBS interference and height dependent Okumura-Hata model. Other factors become less effective.

Fig. 4.13 shows HBS's spectral efficiency curves under the condition of B:3 × 1 × 3

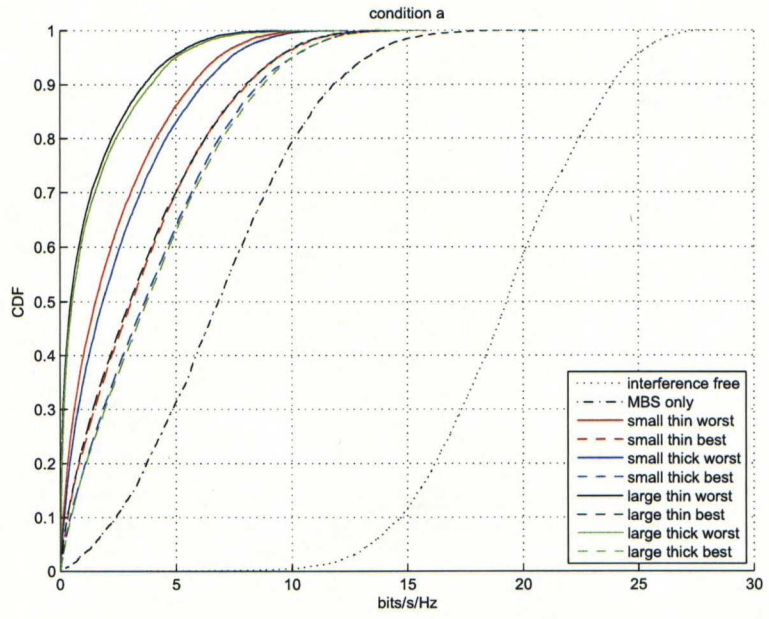

Figure 4.11: DL spectral efficiency under condition (A)

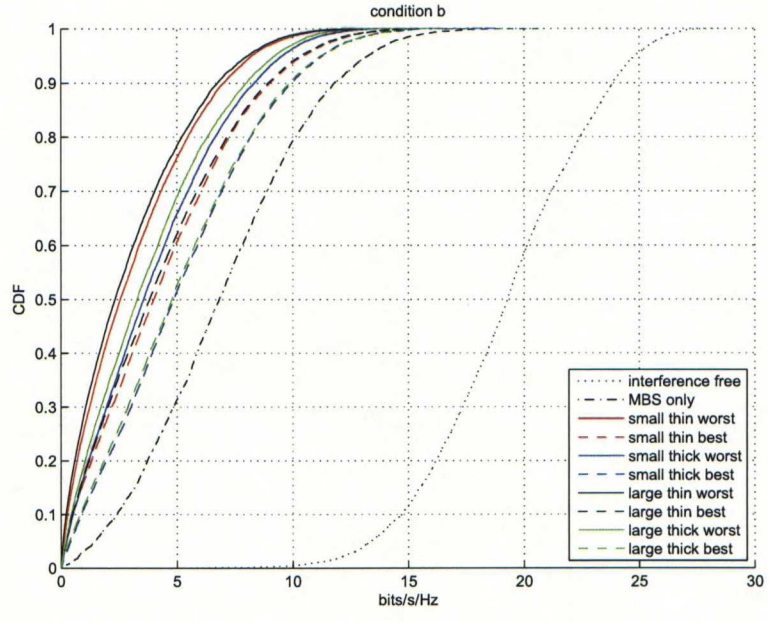

Figure 4.12: DL spectral efficiency under condition (B)

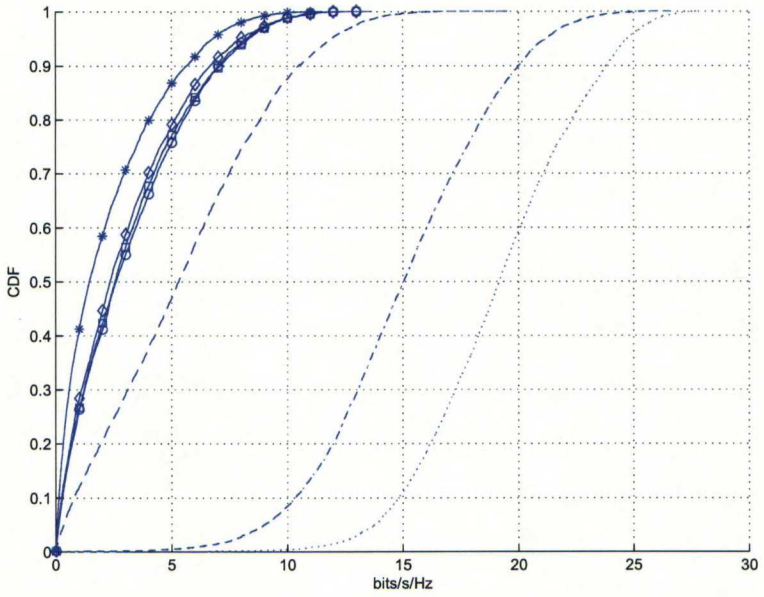

Figure 4.13: DL spectral efficiency with different macrocell distance. Dotted curve: interference free, dashdot curve: MBS interference only with distance 250m, dashed curve: $B:3\times1\times1$ with distance 250m, solid curve with star: $B:3\times1\times3$ with distance 50m, curve with diamond: $B:3\times1\times3$ with distance 150m, curve with square: B:$3\times1\times3$ with distance 250m, curve with circle: B:$3\times1\times3$ with distance 1000m

and thin internal walls with different MBS distances (50m, 150m, 250m, 1000m). In the presence of neighbor's HBSs, the interference from them will dominate and largely restrict the spectral efficiency of our reference HBS. Interference from MBS become indistinctive (only slightly improve due to distance increases). However, by limiting the number of neighbors step by step (first from B:$3\times1\times3$ to B:$3\times1\times1$, and then from $B:3\times1\times1$ to $B:1\times1\times1$), DL spectral efficiency improves dramatically.

4.3 Public safety framework simulations

This section assumes that the emergency UE (EUE) requires three parallel data connection each of 384 kbps in order to setup simultaneous emergency multimedia (image, conversational video, real-time data) sessions resembling that of [29]. In practice, adaptive radio resource management methods may be used to improve performance of the connections and maximize resource utilization efficiency. There-

Table 4.3: Mobile telemedicine service simulation parameters

The number of indoor UEs is 24 for multi-floor apartments block, and 10 for terraced houses. Target uplink load factor of macrocell is 0.5 with other-cell to own-cell interference ratio is 0.5
Indoor path loss is modeled as $98.5 + 20\log_{10}(R) + L_{wall}$ plus a log-normal distributed shadow fading with 4dB standard deviation, where R in km and L_{wall} is 8/15/20dB for light/internal/outer wall respectively. Indoor-to-outdoor path loss is modeled as [33] $PL = Pr(R)PL_{LOS}(R) + (1 - Pr(R))PL_{NLOS}(R) + L_{wall}$, where $PL_{LOS}(R) = 103.8 + 20.9\log_{10}(R)$ $PL_{NLOS}(R) = 145.4 + 37.5\log_{10}(R)$ $Pr(R) = 0.5 - \min(0.5, 5\exp(-0.156/R)) + \min(0.5, 5\exp(-R/0.03))$ plus a log-normal shadow fading with 10dB standard deviation.
The macrocell antenna gain is calculated as $G(\theta) + G_{\max} - \min(12(\frac{\theta}{\theta_{3dB}}), G_s), \quad -\pi \leq \theta \leq \pi$, where $\theta_{3dB} = 70$ degrees, $G_s = 20dB$ and $G_{\max} = 16dB$

fore, by ignoring radio resource management schemes in our simulations, the results presented in this paper provide the lower bound of the achievable EUE performance for both the MBS and FBS cases. Moreover, the EUE retains a high priority by default, meaning its serving BS can only provide voice services to other UE sharing the same resources.

Femtocells are assumed to reuse the same frequency band as macrocells and grant only CSG access to indoor UEs. Simulation parameters including path loss model, antenna model, dimensioning and service parameters are summarized in Table 4.3 and 4.4.

Our simulation compares the CDFs of EUE uplink transmission power in the cases (a) where EUE can be granted access to both MBS and FBSs, (b) where EUE can be only access to FBSs, and (c) where EUE can be only access to MBS. Results also

Table 4.4: Indoor UEs service constitution ratio

	Voice	144kbps data	384kbps data
MUE(100m)	90%	10%	0
MUE(300m)	100%	0	0
HUE	40%	20%	40%
Target Eb/N0	4.5dB	2dB	2dB

show the uplink performance differences between the cases when buildings are within the high data rate service range of MBS and when buildings are at the macrocell edge. The building dimensions are assumed to be B:3 $\times$ 2 $\times$ 8 for MDU structured high-rise building and B:5 $\times$ 1 $\times$ 1 for terraced 2-floor building.

4.3.1 Multi-floor Building

As shown in Fig. 4.14, when P_{femto} equals 0.2 and building distance is 100m, the outage rate of emergency service is kept under 10% since the multi-floor building is within the service coverage area of MBS. As P_{femto} increases, the outage rate is efficiently reduced and eventually under 1% when P_{femto} is 0.8. In the building at cell edge, the emergency service requirement can be fulfilled under 5% outage rate when P_{femto} exceeds 0.5. Because this emergency service is rather coverage limited, MBS can not compensate for the outage event at cell edge.

4.3.2 Terraced Building

Fig. 4.15 shows the corresponding result in terraced building as those in multi-floor building. It is worth noting that the performance gain contributed by femtocells decreases due to the fact that the average path loss between EUE and its serving femtocell is raised for 2 reasons. First, in the case EUE and serving femtocell are in the same 2-floor house, both femtocell and EUE can be resided at any of the floors, which increases both distance dependent path loss and penetration loss. Second, when serving femtocell and EUE reside in different houses, the missing of upper and lower close neighbor reduces the possibility that femtocell is close enough to EUE. As a result, compared with the case in multi-floor building, the increasing amount in EUE outage rate is 1-2% when building distance is 100m and around 5-12% when building is at cell edge.

Fig. 4.16 summarizes EUE outage rate when different P_{femto} are given under the assumption of multi-floor and terraced building respectively. At low P_{femto}, EUE in multi-floor building suffers a densely populated UE environment in comparison with EUE in terraced houses and results in higher outage rates. As P_{femto} increases, the outage rate of EUE in multi-floor building decreases much faster due to the facts

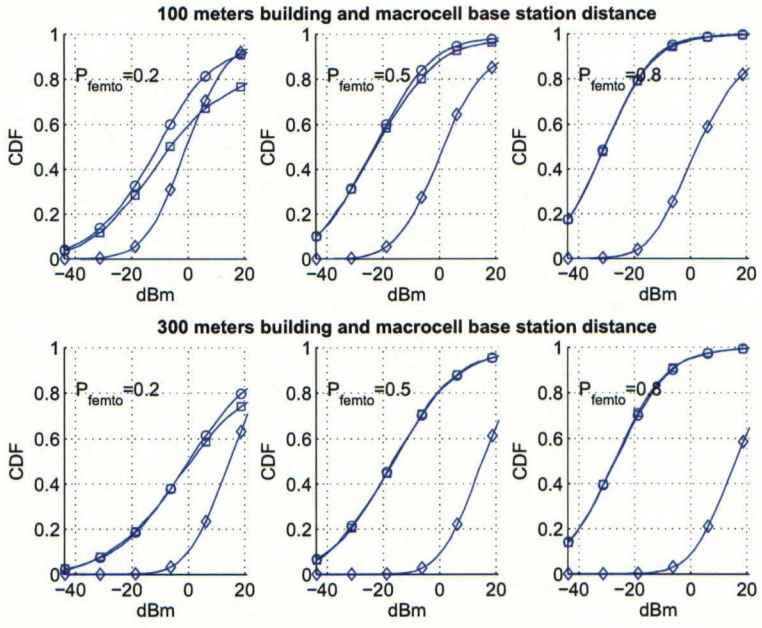

Figure 4.14: CDFs of EUE transmission power in multi-floor apartment block. Line with circle denotes both MBS and FBSs are granted access to EUE. Line with square denotes only FBSs access. Line with diamond denotes only MBS access

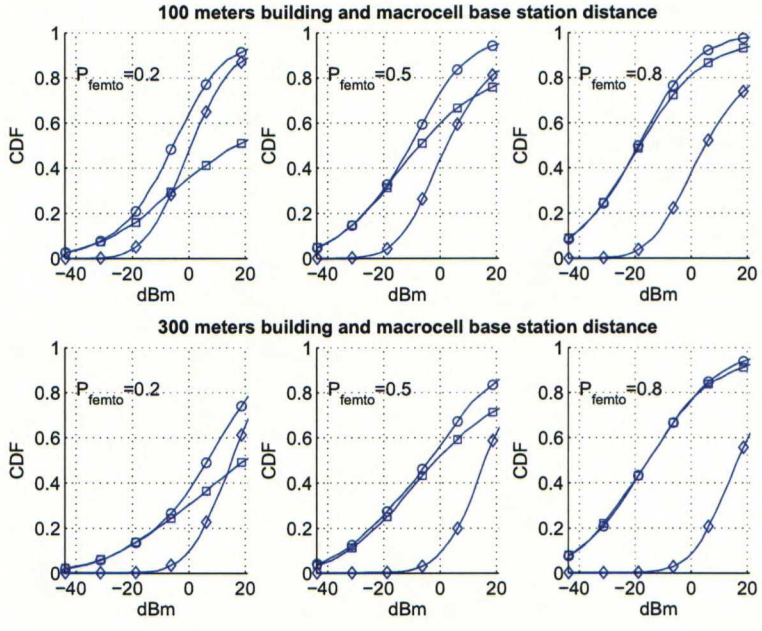

Figure 4.15: CDFs of EUE transmission power in terraced houses. Line with circle denotes both MBS and HBSs are granted access to EUE. Line with square denotes only HBSs access. Line with diamond denotes only MBS access.

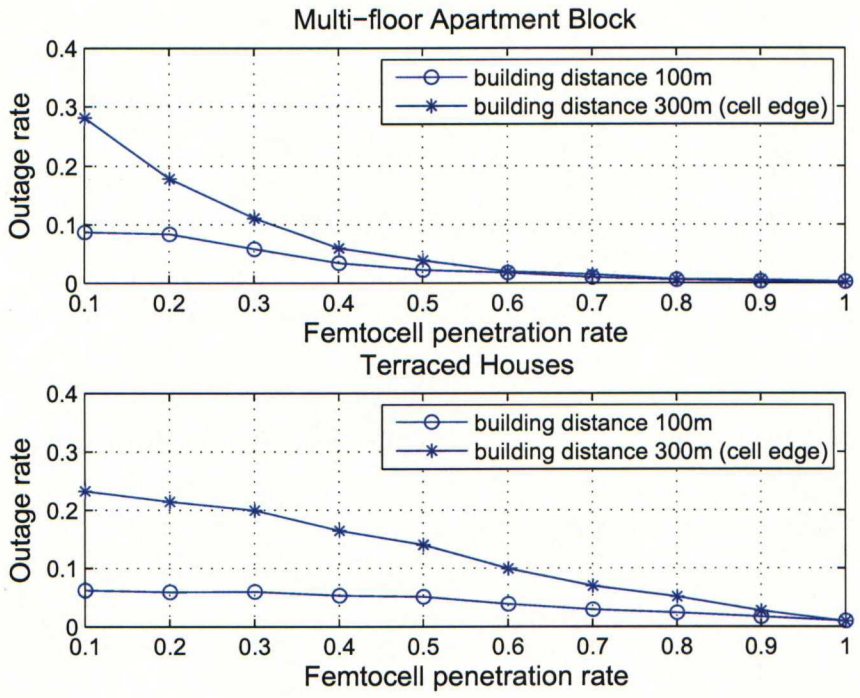

Figure 4.16: Emergency service outage rate with different femtocell penetration ratios

that femtocell reduces average uplink interference from neighbors' and it is more probable that EUE have a serving femtocell nearby in a multi-floor building. It is also noted that the emergency service can be only fulfilled at cell edge when P_{femto} exceeds a threshold (for the emergency service at 95th percentile, P_{femto} 0.43 and 0.8 are needed respectively).

Chapter 5

Interference suppression in closed femtocells: a case study

While at best, femtocells provide significant benefits for mobile operators and users alike, their introduction comes with great many new challenges as stated in Chapter 3. Among these is the interference between macro and femtocells, but also between individual femtocells. Furthermore, the effect of interference needs to be studied separately for downlink and uplink. To mitigate the interference related problems several concepts have been proposed including, but not limited to, open access, dedicated band deployment, transmit power optimization, interference cancellation, adaptive antennas and MIMO schemes.

In the first phase of femtocell deployment closed subscriber group (CSG) configuration is expected to be widely used due to security, billing and contractual concerns. For this reason, it is important to develop methods for alleviating co-channel interference between private femtocells. Here, we present a method for transmit beamforming based interference control utilizing multiple antennas in the FBS in conjunction with a control-only connection established between UE and interfering FBSs. It is shown through analysis and simulations that even simple and practical transmit beamforming methods can be used to effectively suppress the interference in adjacent FBSs.

This chapter is structured as follows: section 5.1 discusses the general system model and corresponding assumptions. Investigated transmit beamforming methods are described in section 5.2 and the performance analysis is outlined in section 5.3.

5.1 System Model

Interference scenario

We consider the interference case where *downlink co-channel interference occurs between adjacent femtocells* as listed in [20]. We have limited the number of femtocells to two because due to building structures downlink interference is often characterized by one dominant neighboring femtocell, as discussed in the previous chapter. Furthermore, we assume that transmission power in FBSs is constant and handover is not allowed. This is interesting and relevant scenario especially in blocks of flats environment where FBSs may operate on the same carrier in adjacent private households and CSG configuration is applied. We have an illustrative example in Fig. 5.1 where interference takes place between two adjacent femtocells. It is assumed that upper and lower flats are separated by a single wall (midmost horizontal wall in Fig. 5.1) and location selection for the FBS 1 and 2 is done independently. In depicted situation users 2a and 2b in upper flat admit a good channel towards serving FBS (FBS number 2) but in lower flat user is located in the room where interference from FBS 2 may dominate over the signal from serving FBS 1. We emphasize that the mean SINR in terminal 1 depends on the building structures: In the case whereby the wall separating the flats is a load-bearing wall, different rooms are separated by light walls and doors are open, then signal from serving FBS may dominate over the interference in the whole household.

Adopted assumptions

We have adopted the following assumptions regarding the general framework:

(A1) We focus on a two-cell scenario where adjacent FBS create downlink co-channel interference to UE of the reference cell. Transmission power in FBSs is constant and handover between cells is not possible, *i.e.* CSG configuration is applied but *UE can form a control connection to both serving and interfering FBS.*

(A2) There are M transmit antennae in both FBSs and single receive antenna in a UE. Terminal can estimate signals from different antennas of both serving and interfering FBSs. Channel estimation is assumed to be perfect. Terminal may send

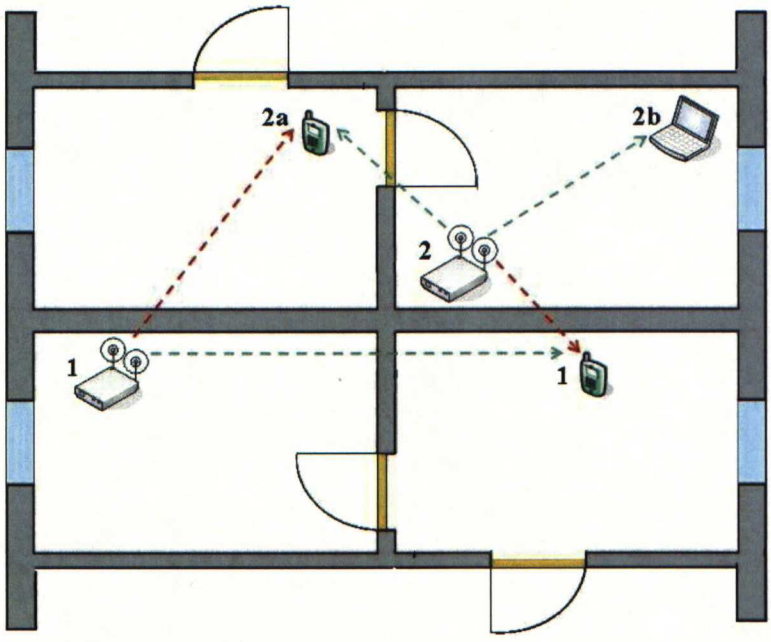

Figure 5.1: Illustration of an interference scenario between femtocells. Channel between FBS 2 and its users is good while user 1 connected to FBS 1 may face heavy interference.

a feedback message to the both femto transceivers including information for antenna weight selection.

(A3) Channels related to different antennas of the same FBS are *i.i.d.* complex zero-mean Gaussian, while mean transmission power is different for separate FBSs. Fast fading in different FBSs is uncorrelated.

Let us briefly discuss on the validity of assumptions. The interference scenario of (A1) is well valid for e.g. HSDPA case because first home femto deployments employ HSDPA. Moreover, due to constraints in spectrum availability, it is not attractive for operators to dedicate more than one carrier for femto operations. Also usage of fixed transmission power and CSG are expected in many deployments while control connection to adjacent BSs is currently possible only in macrocell systems. Yet, this extension to the current femtocell capabilities is the main research question: how much benefit can be accrued by establishing a control connection to the interfering adjacent FBS?

We note that our discussion focus on benefits from transmit beamforming control

over adjacent femtocells when downlink transmission power is fixed. Yet, it is known from [23] that the adjustable transmission power in femtocells is a good option although it may lead to either undesired power competition between households or coverage problems if FBS transmission power is allowed to decrease excessively. Thus, self-organizing femtocells with feasible combination of power control and interference suppression ability is a good topic for future work.

In order to keep the discussion on generic level we have adopted in (A2) the M transmit antenna assumption although two-antenna approach is currently more feasible because in, for example HSDPA, transmit beamforming is defined for two antennas. Yet, in LTE there will be a support also for four-antenna transmit beamforming methods [34]. Legacy HSDPA terminals are equipped with one receive antenna and they can estimate channels of two different BS antennae from primary common pilot channels (P-CPICHs) and define the beamforming feedback that is then send to BS through a dedicated feedback channel. For handover purposes HSDPA terminal is also able to estimate P-CPICH signals from adjacent BSs and thus, it is able to define related beamforming feedback for adjacent BSs. Actually in WCDMA soft handover terminal defines the beamforming feedback that best fits to transmission from BSs in the so-called active set [35].

The channel statistics may vary depending on the building structures but due to rich scattering the Rayleigh fading assumption of (A3) is a good approximation although it fails when there is line-of-sight between transmitter and receiver. However, since Rayleigh fading statistics do not favor transmit beamforming then they can be used to evaluate lower bounds for the performance of the investigated methods. The mean transmission power from different FBSs is not the same due to locations in separate apartments but antenna correlations of the same FBS may occur in practice. Yet, correlation is usually small and can be ignored when rich scattering around the FBS takes place.

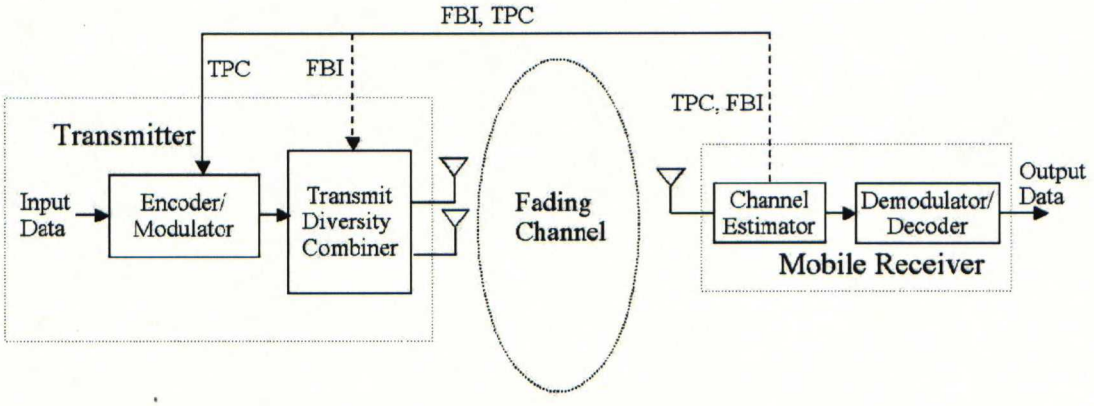

Figure 5.2: General system structure for UTRA FDD downlink with feedback.

5.2 Transmit beamforming and interference suppression

5.2.1 Preliminaries

We focus on the usage of transmit antenna selection as a part of the interference suppression method because it provides a lower bound for the reachable gain from proposed approach and also allows simple closed-form analysis where the impact of different parameters is comprehensive to the reader. Antenna selection is also quite practical due to small signaling overhead.

5.2.2 Transmit beamforming

We start by recalling the transmit beamforming of HSDPA. As depicted in Fig. 5.2 the receiver encodes channel state information (CSI) into the feedback message that is transmitted using feedback indicator (FBI) field in uplink channel. Similarly, transmit power control (TPC) commands are passed in the TPC field. Note that the transmit power control that compensates fast fading is used in downlink only for services with strict latency requirements like circuit-switched voice, while data services mostly employ HS-DSCH where TPC is not present.

Assume an interference free case. Then the received signal in the terminal is of the

form

$$r = (\mathbf{h} \cdot \mathbf{w})s + n = \Big(\sum_{m=1}^{M} w_m h_m \Big) s + n, \tag{5.1}$$

where s is the transmitted symbol, $\mathbf{h} = (h_1, \ldots, h_M)$ consists of complex zero-mean Gaussian channel coefficient, n refers to additive white Gaussian noise, and vector $\mathbf{w} \in \mathbf{W}$ refers to the codebook of complex transmit beamforming weights such that $||\mathbf{w}|| = \mathbf{1}$. Given received signal (5.1) and quantization set $\mathbf{W}$, the weight $\widehat{\mathbf{w}}$ that maximizes SNR in reception can be found after evaluating (5.1) for all weight vectors. Thus, for given channel coefficient vector $\mathbf{h}$ the applied weight $\hat{\mathbf{w}}$ is found after solving the finite dimensional optimization problem

$$\text{Find } \widehat{\mathbf{w}} \in \mathbf{W}: \quad |\mathbf{h} \cdot \widehat{\mathbf{w}}| = \max_{\mathbf{w} \in \mathbf{W}} |\mathbf{h} \cdot \mathbf{w}|. \tag{5.2}$$

In antenna selection method $\mathbf{W}$ consists of M vectors of the form $\mathbf{w} = (0, \ldots, 0, 1, 0, \ldots, 0)$, where the non–zero component indicates the best channel in terms of the received power. We note that feedback overhead during each update is $2\lceil \log_2(M) \rceil$ bits for antenna selection. The actual feedback capacity need depends on the update rate which is decided in system design based on expected fading rate due to terminal mobility. In HSDPA the update rate is 1.5kbps.

5.2.3 Interference suppression

In the following we assume a scenario consisting of one desired user and a dominant interferer. SNR received by kth user from lth femto transmitter is denoted by

$$\gamma_{l \to k} = \bar{\gamma}_{l \to k} |\mathbf{h}_{l \to k} \cdot \widehat{\mathbf{w}}_{l \to l}|^2,$$

where $\bar{\gamma}_{l \to k}$ is the mean SNR in the link. We note that in conventional transmit beamforming the weight is selected according to (5.2) and it maximizes SNR when $k = l$ *i.e.*, when transmission is directed to the dedicated femto user. Since vector channels $\mathbf{h}_{l \to l}$ and $\mathbf{h}_{l \to k}$ are uncorrelated the interference $\mathbf{h}_{l \to k} \cdot \widehat{\mathbf{w}}_{l \to l}$ is zero-mean Gaussian.

When transmit beamforming is applied and there are two FBS and two terminals, the signal to interference and noise ratios (SINRs) in first and second UE are given

by

$$\begin{aligned}\Upsilon_1 &= \frac{\gamma_{1\to 1}}{1+\gamma_{2\to 1}} = \frac{\bar{\gamma}_{1\to 1}|\mathbf{h}_{1\to 1}\cdot\widehat{\mathbf{w}}_{1\to 1}|^2}{1+\bar{\gamma}_{2\to 1}|\mathbf{h}_{2\to 1}\cdot\widehat{\mathbf{w}}_{2\to 2}|^2},\\ \Upsilon_2 &= \frac{\gamma_{2\to 2}}{1+\gamma_{1\to 2}} = \frac{\bar{\gamma}_{2\to 2}|\mathbf{h}_{2\to 2}\cdot\widehat{\mathbf{w}}_{2\to 2}|^2}{1+\bar{\gamma}_{1\to 2}|\mathbf{h}_{1\to 2}\cdot\widehat{\mathbf{w}}_{1\to 1}|^2}.\end{aligned} \tag{5.3}$$

Due to (A1) handover between FBSs is not allowed and either of the FBSs may dominate. To track this we denote the mean SNR ratios by

$$\nu_1 = \bar{\gamma}_{1\to 1}/\bar{\gamma}_{2\to 1}, \quad \nu_2 = \bar{\gamma}_{2\to 2}/\bar{\gamma}_{1\to 2}.$$

If femtocells are well separated then both ν_1 and ν_2 are large and interference is negligible. On the other hand, extreme cases exists where both ν_1 and ν_2 are small, see [19]. However, such situations are rare and in most of the cases at least one of the ratios is large.

Let us adopt the most common interference situation where either of the two links admit a good channel. For simplicity we assume that user in first (reference) femtocell suffers from interference originating from second femtocell, but user in second femtocell admit a good channel *i.e.*, $\nu_2 >> 1$. In the applied interference suppression method we allow the user terminal in first femtocell to establish a control channel connection with interfering FBS according to (A1) and (A2). Then interfered terminal can request second FBS to replace $\widehat{\mathbf{w}}_{2\to 2}$ by the weight $\check{\mathbf{w}}_{2\to 1}$ that is selected using the criteria

$$\text{Find } \check{\mathbf{w}}_{2\to 1} \in \mathbf{W}: \quad |\mathbf{h}_{2\to 1}\cdot\check{\mathbf{w}}_{2\to 1}| = \min_{\mathbf{w}\in\mathbf{W}} |\mathbf{h}_{2\to 1}\cdot\mathbf{w}|. \tag{5.4}$$

This approach will minimize the interference term in Υ_1 of (5.3) while the user terminal in second femtocell will loose gain from transmit beamforming because $\check{\mathbf{w}}_{2\to 1}$ is selected independently from the channel $\mathbf{h}_{2\to 2}$. Given that $\nu_2 >> 1$ it is expected that loosing beamforming gain is not critical for user of the second femtocell. In practice FBS may probe the interference situation in its cell by requesting reports from users that it is serving. If received signal strengths are well sufficient for served terminals, then it may apply available transmit beamforming methods to decrease the interference level in adjacent cell provided that this operation is not violating connections of its own users.

The SINR formulae of (5.3) are now given by

$$\begin{aligned}\Upsilon_{(1)} &= \frac{\hat{\gamma}_{1\to1}}{1+\check{\gamma}_{2\to1}} = \frac{\bar{\gamma}_{1\to1}|\mathbf{h}_{1\to1}\cdot\widehat{\mathbf{w}}_{1\to1}|^2}{1+\bar{\gamma}_{2\to1}|\mathbf{h}_{2\to1}\cdot\check{\mathbf{w}}_{2\to1}|^2},\\ \Upsilon_{(2)} &= \frac{\tilde{\gamma}_{2\to2}}{1+\tilde{\gamma}_{1\to2}} = \frac{\bar{\gamma}_{2\to2}|\mathbf{h}_{2\to2}\cdot\check{\mathbf{w}}_{2\to1}|^2}{1+\bar{\gamma}_{1\to2}|\mathbf{h}_{1\to2}\cdot\widehat{\mathbf{w}}_{1\to1}|^2}.\end{aligned} \tag{5.5}$$

Here weights $\widehat{\mathbf{w}}_{1\to1}$ and $\check{\mathbf{w}}_{2\to1}$ are selected according to (5.2) and (5.4), leading to SNRs $\hat{\gamma}_{1\to1}$ and $\check{\gamma}_{2\to1}$ of dedicated and suppressed signals. Notations $\tilde{\gamma}_{2\to2}$ and $\tilde{\gamma}_{1\to2}$ refer to signal SNRs in cases where transmit beamforming weights are selected independently from the channels. Finally, SINR subscripts are in parenthesis to emphasize the fact that first user is preferred when defining beamforming weights.

An approach similar to (5.5) was previously used in case of a single cell multiuser scheduling and two antennas [36], [37]. There a BS applies orthogonal weight vectors to suppress the own cell interference when simultaneous transmission to two users is executed. When number of users in scheduling queue is large the BS scheduler may find user pair with roughly orthogonal channels and the method provides gain in terms of cell throughput. In case of a femtocell system terminal receives interference from adjacent FBS and the user selection or use of orthogonal weights not provide similar benefits to the BS case. Therefore, to inform the weight $\check{\mathbf{w}}_{2\to1}$ for interference suppression an additional control channel is needed between terminal and interfering FBS.

5.3 Performance analysis

Given the proposed method defined by (5.5), we now proceed with the system performance analysis employing both the cumulative distribution function (CDF) of SINR as well as outage and average rates.

5.3.1 Cumulative distribution function for SINR

In order to derive the CDF of the SINR, we must first determine the outage and average rate using the expressions for the SINR based on (5.3) and (5.5). Suppose we define a function of random variables Z as follows:

$$Z = \frac{X}{1+Y},$$

where X and Y are independent random variables. It follows that the CDF of Z, $F_Z(z)$, is then defined by [38]:

$$F_Z(z) = \int_1^{\infty} F_X(zt) f_Y(t-1) dt, \tag{5.6}$$

where f_Y is the probability distribution function (PDF) of Y and $F_X(x)$ is the CDFs of X.

Suppose now we consider the distribution of $\Upsilon_{(1)}$ when antenna selection is selected as the transmit beamforming method. According to (5.2), (5.4) and (A3) variables $\hat{\gamma}_{1\to 1}$ and $\check{\gamma}_{2\to 1}$ are then defined as a maximum and minimum values over M independent exponentially distributed variables. Consequently, we obtain the following expressions:

$$\begin{aligned} F_{\hat{\gamma}_{1\to 1}}(\gamma) &= \left(1 - e^{-\gamma/\bar{\gamma}_{1\to 1}}\right)^M, \\ F_{\check{\gamma}_{2\to 1}}(\gamma) &= \left(e^{-\gamma/\bar{\gamma}_{2\to 1}}\right)^M, \ \gamma > 0 \end{aligned}$$

which after differentiation we find that the corresponding PDFs are of the form:

$$\begin{aligned} f_{\hat{\gamma}_{1\to 1}}(\gamma) &= \frac{M e^{-\gamma/\bar{\gamma}_{1\to 1}}}{\bar{\gamma}_{1\to 1}} \left(1 - e^{-\gamma/\bar{\gamma}_{1\to 1}}\right)^{M-1}, \\ f_{\check{\gamma}_{2\to 1}}(\gamma) &= \frac{M e^{-M\gamma/\bar{\gamma}_{2\to 1}}}{\bar{\gamma}_{2\to 1}}, \ \gamma > 0. \end{aligned} \tag{5.7}$$

Thus, in order to compute the CDF of $\Upsilon_{(1)}$, we recall expression for $F_{\hat{\gamma}_{1\to 1}}$ as:

$$F_{\hat{\gamma}_{1\to 1}}(\gamma) = \sum_{m=0}^{M} \binom{M}{m} (-1)^m e^{-m\gamma/\bar{\gamma}_{1\to 1}}, \tag{5.8}$$

where binomial series expansion has been applied. After combining equations (5.6) and (5.8) together, we then determine that

$$\begin{aligned} F_{\Upsilon_{(1)}}(\gamma) &= \sum_{m=0}^{M} \binom{M}{m} (-1)^m \frac{M e^{\frac{M}{\bar{\gamma}_{2\to 1}}}}{\bar{\gamma}_{2\to 1}} \int_1^{\infty} e^{-\frac{tM}{\bar{\gamma}_{2\to 1}} - \frac{tm\gamma}{\bar{\gamma}_{1\to 1}}} dt \\ &= \sum_{m=0}^{M} \binom{M}{m} \frac{(-1)^m \cdot \nu_1 \cdot M}{\nu_1 \cdot M + m\gamma} e^{-m\gamma/\bar{\gamma}_{1\to 1}}. \end{aligned} \tag{5.9}$$

We can then obtain $F_{\Upsilon_{(2)}}$ from (5.9) by replacing ν_1 by ν_2, $\bar{\gamma}_{1\to 1}$ by $\bar{\gamma}_{2\to 2}$ and setting $M = 1$, thus yielding:

$$F_{\Upsilon_{(2)}}(\gamma) = 1 - \frac{\nu_2}{\nu_2 + \gamma} e^{-\gamma/\bar{\gamma}_{2\to 2}}. \tag{5.10}$$

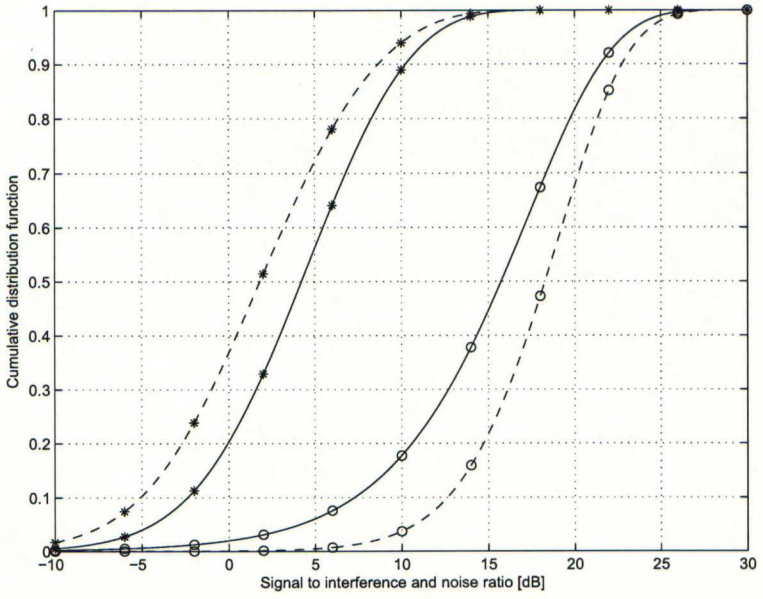

Figure 5.3: Cumulative distribution function for Υ_1 (dashed curve, '*'), Υ_2 (dashed curve, 'o'), $\Upsilon_{(1)}$ (solid curve, '*') and $\Upsilon_{(2)}$ (solid curve, 'o') when antenna selection over two antennas is applied. Mean SNRs are $\bar{\gamma}_{1\to1} = 10\text{dB}$, $\bar{\gamma}_{2\to2} = 20\text{dB}$, $\bar{\gamma}_{2\to1} = 10\text{dB}$ and $\bar{\gamma}_{1\to2} = 0\text{dB}$.

Moreover, if antenna selection is performed independently across separate cells, we can then employ (5.9) in a similiar approach in order to obtain the following result:

$$F_{\Upsilon_k}(\gamma) = \sum_{m=0}^{M} \binom{M}{m} \frac{(-1)^m \cdot \nu_k}{\nu_k + m\gamma} e^{-m\gamma/\bar{\gamma}_{k\to k}}. \tag{5.11}$$

Given the CDF value or SINR, equations (5.9)–(5.11) can be used to investigate the impact of different parameters such as mean SNRs and number of antennas. For example, while designing the decision threshold for usage of proposed method the performance degradation can be calculated from (5.10), (5.11) while expected gain is obtained from (5.9), (5.11).

Suppose we consider the numerical example where the network supports a dedicated signal in first femtocell that possesses a relatively good signal strength (e.g., $\bar{\gamma}_{1\to1} = 10\text{dB}$) but an interfering signal originating from the adjacent femtocell is also strong (e.g., $\bar{\gamma}_{2\to1} = 10\text{dB}$). Simultaneously, a second signal being served by the FBS also possesses a good signal strength ($\bar{\gamma}_{2\to2} = 20\text{dB}$) while the strength of an interfering signal is weak ($\bar{\gamma}_{1\to2} = 0\text{dB}$). This scenario is illustrated in Fig. 5.1.

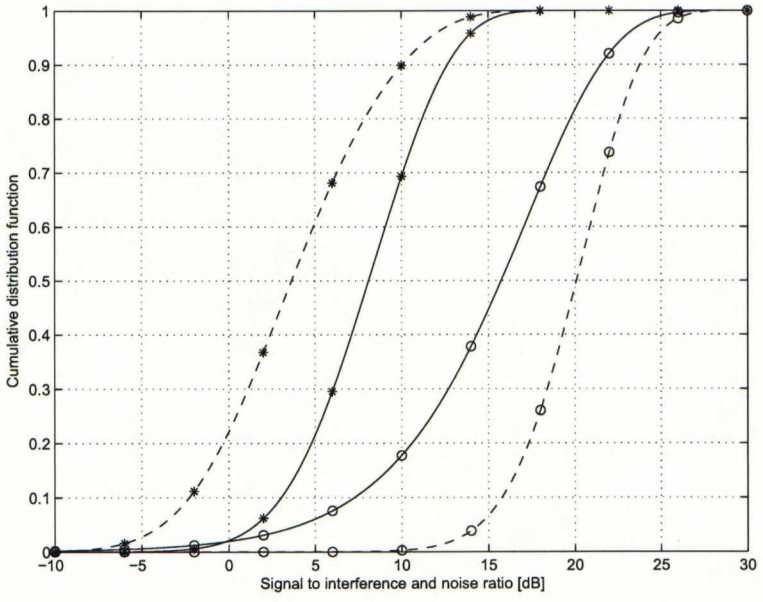

Figure 5.4: Cumulative distribution function for Υ_1 (dashed curve, '*'), Υ_2 (dashed curve, 'o'), $\Upsilon_{(1)}$ (solid curve, '*') and $\Upsilon_{(2)}$ (solid curve, 'o') when antenna selection over four antennas is applied. Mean SNRs are $\bar{\gamma}_{1\to1}$ = 10dB, $\bar{\gamma}_{2\to2}$ = 20dB, $\bar{\gamma}_{2\to1}$ = 10dB and $\bar{\gamma}_{1\to2}$ = 0dB.

The resulting SINR performance based on the aforementioned scenario is given for the case of two antennas in Fig. 5.3 as well as for the case of four antennas in Fig. 5.4. The dashed curves in these figures illustrate the SINR performance when cells operate separately while solid curves denote the situation when proposed interference suppression is applied. Fig. 5.3 shows that even with two antennas the proposed method improves the SINR performance of the transmission links by more than 3dB (up to 70th percentile of the CDF) in the first cell while SINR simultaneously remains at an acceptable level in second cell despite having it use its antenna resources to mitigate interference in the first cell. Furthermore, from Fig. 5.4 it is observed that the four-antenna extension of antenna selection yield up to a 5dB increase in the SINR at the 10th percentile of the CDF in the first cell with a corresponding decrease in the SINR second cell. Consequently, the proposed interference suppression method can be effectively used to share radio resources in a more fair manner between adjacent femtocells, although transmission power in FBSs are fixed and the communications between FBSs is non-existent.

5.3.2 Outage rate

It is also worthwhile to investigate the system performance in terms of outage rate. Suppose we define the outage rate by the expression:

$$R^{\text{out}}(P_{\text{out}}) = A \cdot \log_2\left(1 + B \cdot \gamma(P^{\text{out}})\right), \tag{5.12}$$

where $\gamma(P_{\text{out}})$ is the SINR needed to achieve given outage probability P^{out}, and the parameters A and B are the bandwidth and SNR efficiency factors used to fit the rate of the system with the set of adaptive modulation and coding curves obtained via system simulations. For example, it has been shown that values $A = 0.88$ and $B = 1/1.25$ provide a good fit with the set of LTE adaptive modulation and coding curves [39]. In this paper, we shall set the values $A = B = 1$ in order to provide the upper bound for the system transmission rate.

With respect to the value of $\gamma(P^{\text{out}})$, this can be obtained by obtaining the solution for the following equation:

$$\begin{aligned} P^{\text{out}} &= P\left(\log_2(1+\gamma) < R_0\right) \\ &= \int_0^{\gamma_{R_0}} f_\Upsilon(\gamma)d\gamma = F_\Upsilon(\gamma_{R_0}). \end{aligned} \tag{5.13}$$

In this case, $\gamma_{R_0} = 2^{R_0} - 1$ is the SINR related to limit rate R_0 and, in case of antenna selection formula for F_Υ, it is given by (5.9), (5.10) or (5.11) depending on the employed approach. We note that for a given P^{out} the solution of (5.13) can be computed numerically.

In Fig. 5.5, the outage rates R_1^{out} and $R_{(1)}^{\text{out}}$ are defined as functions of $\bar{\gamma}_{2\to1}$ when $P^{\text{out}} = 0.1$ and SNR value of the serving FBS is 10dB. Comparing the curves in Fig. 5.5 shows that the strength of the interference signal originating from adjacent cell can be adequately attenuated by the proposed approach. Based on the results, transmit antenna selection is capable of significantly improving the link rates. This is particular true of the four-antenna configuration, which provides an efficient tool for removing the interference. When comparing a system that employs this method with another system that does not use transmit beamforming, the gain is extremely large.

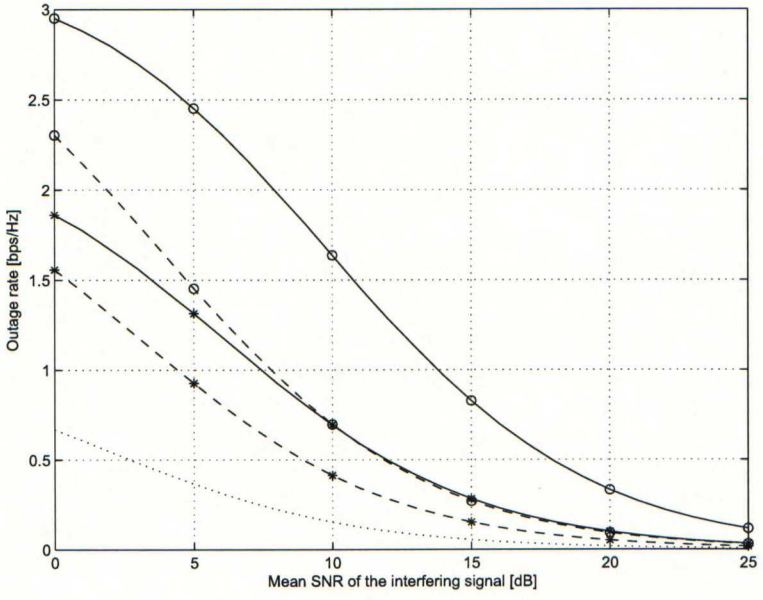

Figure 5.5: The outage rate without transmit beamforming (dotted curve), R_1^{out} (dashed curves) and $R_{(1)}^{\text{out}}$ (solid curves) as a function of $\bar{\gamma}_{2\to 1}$ when antenna selection over two (*) and four (o) antennas is used. The outage probability is 0.1 and mean SNR of the serving cell signal ($\bar{\gamma}_{1\to 1}$) is 10dB.

Observing the outage probability performance as a function of $\bar{\gamma}_{2\to 1}$ when target rate requirement is fixed, we see in Fig. 5.6 for a target rate set to 1.0 bits/s/Hz and the SNR value from the serving FBS equal to 10dB that employing the proposed method significantly decreases the outage probability, especially when transmit beamforming is not applied.

5.3.3 Average rate

Another metric for assessing the performance enhancements offered by the proposed methods is the average rate, which can be computed from the following formula:

$$R^{\text{av}}(\bar{\gamma}_{k\to k}|\bar{\gamma}_{l\to k}) = \int_0^\infty f_\Upsilon(\gamma)\log_2(1+\gamma)d\gamma$$

which is a function of the SNR value of the serving cell and conditioned upon the SNR value of the interfering signal. Therefore, using integrating by parts, we obtain the following:

$$R^{\text{av}}(\bar{\gamma}_{k\to k}|\bar{\gamma}_{l\to k}) = \log_2(e)\int_0^\infty \frac{1-F_\Upsilon(\gamma)}{1+\gamma}d\gamma.$$

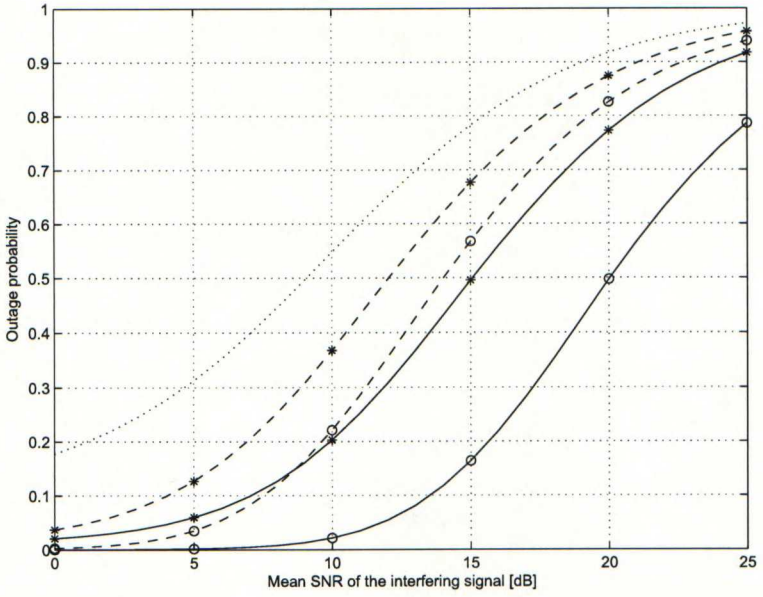

Figure 5.6: The outage probability without transmit beamforming (dotted curve), with two-antenna selection (*) and with four-antenna selection (o) when interference suppression is on (solid curves) and off (dashed curves). The outage rate is set to 1.0 bps/Hz and mean SNR of the serving cell signal ($\bar{\gamma}_{1\to 1}$) is 10dB.

If the proposed interference suppression technique is employed, we then have according to (5.9) the following expression:

$$\int_0^\infty \frac{1-F_{\Upsilon_{(1)}}(\gamma)}{1+\gamma}d\gamma = \sum_{m=1}^{M}\binom{M}{m}\int_0^\infty \frac{(-1)^{m-1}e^{-m\gamma/\bar{\gamma}_{1\to 1}}d\gamma}{(1+\gamma)(1+\frac{m}{\nu_1 M}\gamma)}.$$

In order to compute the integral on the right side of this equation, we apply the following decomposition:

$$\frac{1}{(1+\gamma)(1+\frac{m}{\nu_1 M}\gamma)} = \frac{1}{1-\frac{m}{\nu_1 M}}\left(\frac{1}{1+\gamma} - \frac{\frac{m}{\nu_1 M}}{1+\frac{m}{\nu_1 M}\gamma}\right).$$

Thus, after combining last two equations we obtain a sum of two integrals in which we substitute $t = 1+\gamma$ and $t = 1+\frac{m}{\nu_1 M}\gamma$. Consequently, the resulting integrals yield expressions that are in terms of exponential integral function ([40], (5.1.4))

$$\int_0^\infty \frac{e^{-m\gamma/\bar{\gamma}_{1\to 1}}d\gamma}{1+\gamma} = e^{\frac{m}{\bar{\gamma}_{1\to 1}}}E_1\left(\frac{m}{\bar{\gamma}_{1\to 1}}\right),$$
$$\frac{m}{\nu_1 M}\int_0^\infty \frac{e^{-m\gamma/\bar{\gamma}_{1\to 1}}d\gamma}{1+\frac{m}{\nu_1 M}\gamma} = e^{\frac{M}{\bar{\gamma}_{2\to 1}}}E_1\left(\frac{M}{\bar{\gamma}_{2\to 1}}\right).$$

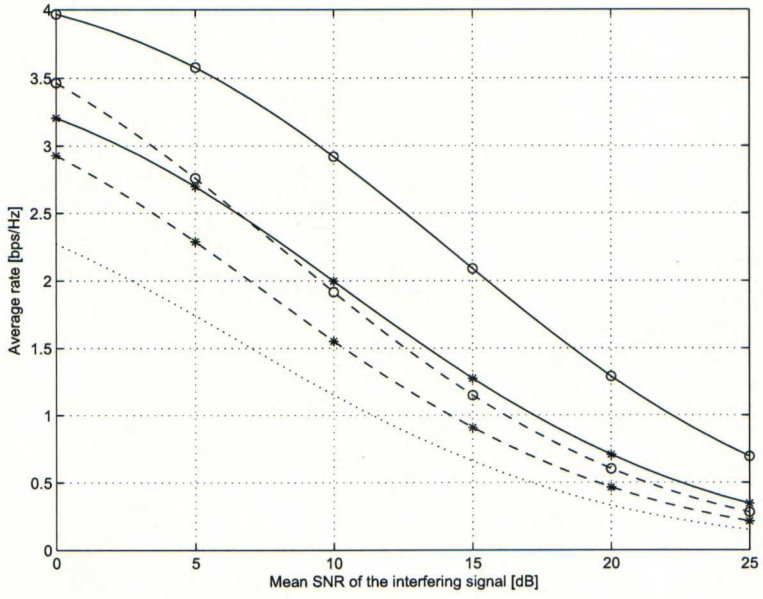

Figure 5.7: The average rate without transmit beamforming (dotted curve), with two-antenna selection (*) and with four-antenna selection (o) when interference suppression is on (solid curves) and off (dashed curves). The mean SNR of the serving cell signal ($\bar{\gamma}_{1\to 1}$) is 10dB.

Thus, the average rate in this case is given by:

$$R_{(1)}^{\mathrm{av}}(\bar{\gamma}_{1\to 1}|\bar{\gamma}_{2\to 1}) = \log_2(e)\sum_{m=1}^{M}\binom{M}{m}(-1)^{m-1}\cdot A_m, \tag{5.14}$$

where

$$A_m = \frac{1}{1-\frac{m}{\nu_1 M}}\left(e^{\frac{m}{\bar{\gamma}_{1\to 1}}}E_1\left(\frac{m}{\bar{\gamma}_{1\to 1}}\right) - e^{\frac{M}{\bar{\gamma}_{2\to 1}}}E_1\left(\frac{M}{\bar{\gamma}_{2\to 1}}\right)\right).$$

It is assumed that $\bar{\gamma}_{1\to 1} \neq \frac{m}{M}\bar{\gamma}_{2\to 1}$. Furthermore, based on the exponential integral functions employed in this derivation, we observe the following:

$$A_m = e^{\frac{m}{\bar{\gamma}_{1\to 1}}}E_2\left(\frac{m}{\bar{\gamma}_{1\to 1}}\right),\ \bar{\gamma}_{1\to 1} = \frac{m}{M}\bar{\gamma}_{2\to 1}, \tag{5.15}$$

Note that the average rate $R_{(2)}^{\mathrm{av}}$ for second user is obtained from (5.14) after setting $M = 1$ and replacing ν_1 by ν_2, $\bar{\gamma}_{1\to 1}$ by $\bar{\gamma}_{2\to 2}$ and $\bar{\gamma}_{2\to 1}$ by $\bar{\gamma}_{1\to 2}$.

If the links in the adjacent cells are operated independently, we can then use the CDF (5.11) from the previous calculation. Consequently, the resulting transmission

rate (5.14) can now be expressed as:

$$A_m = \begin{cases} \frac{1}{1-\frac{m}{\nu_k}} \left(e^{\frac{m}{\bar{\gamma}_{k\to k}}} E_1 \left(\frac{m}{\bar{\gamma}_{k\to k}} \right) - e^{\frac{1}{\bar{\gamma}_{l\to k}}} E_1 \left(\frac{1}{\bar{\gamma}_{l\to k}} \right) \right), \\ e^{\frac{1}{\bar{\gamma}_{l\to k}}} E_1 \left(\frac{1}{\bar{\gamma}_{l\to k}} \right), \ \bar{\gamma}_{l\to k} = \frac{\bar{\gamma}_{k\to k}}{m}. \end{cases}$$

The resulting average rates produce by system employing the proposed method are illustrated in Fig. 5.7, where strength of the desired signal is set to 10dB and SNR value of the interfering signal from adjacent cell is increased to 25dB. The observed results confirm previously stated trend, namely the proposed interference suppression method will greatly enhance the systems immunity against co-channel interference.

Chapter 6

Conclusions and future work

6.1 Conclusions

In this thesis the concept of femtocell was introduced. An overview of the major motivation to this concept was presented. This study assumes HSPA as the underlying radio interface used by femtocell base station. Based on the current 3GPP standard, femtocell extends the service coverage of UMTS cellular networks to indoor environment, and creates high-throughput hotspot due to its small coverage nature and restricted accessibility. As we focus on the radio access aspect of femtocell, the signal model framework set by HSPA is investigated as a basis for study. We also introduce the concepts of UTRAN network architecture and radio interface protocols.

The attractivity of the femtocell concept is the result of continuous cell micro-ization process. With a reduced cell size, the area spectral efficiency increases an order of magnitude compared with traditional macrocellular networks, because the average transmission power of terminals and base stations are reduced in the femtocell-deployed area. Meanwhile, due to its uncoordinated property, a massive femtocell deployment also introduce additional interference problems related to other femtocells and macrocells. Possible technical solutions from previous studies are investigated and reviewed.

After identifying the potential interference scenarios, femtocell case studies are carried out based on system-level simulations. In uplink, the impact of building dimensions and windows are studied. The performance of femtocell under three different

spectral usage schemes is compared. The uplink outage rate is extracted from statistical results for different building block dimensions and for various wall attenuation properties. In downlink, the throughput is evaluated for femtocell usage.

This thesis also covers the femtocell use case related to emergency telemedicine service through femtocellular network. This use case is supported by simulations carried out in two types of MDU building structures. Results shows that femtocells give a significant performance advantage compared with traditional macrocell use case.

When employing closed subscriber group configurations in femtocell deployment, where general handovers are not permitted between femtocell base stations, the signal strength of the interference can become unacceptably high due to the lack of coordination between base stations. Consequently, we propose a practical interference suppression method based on transmit beamforming with antenna selection that can be used to mitigate the downlink co-channel interference from uncoordinated adjacent femtocell base stations.

The performance analysis conducted in this work was based on both mathematical derivations and simulations measures for the performance were the cumulative distribution function for SINR, the outage rate, and the average rate. Performance results for all measures showed the same trend, namely, the proposed method is capable of achieving a substantially high suppression of the interference originating from adjacent femtocells. The drawback is that if the transmit antenna resources are used to suppress the interference in adjacent cells, the the beamforming gain in target cell is lost. Nevertheless, in practice this is only a problem if both of the femtocells under investigation are suffering from heavy interference.

6.2 Future work

The thesis assumes that base stations have a fixed downlink transmission power. In practice, both macro- and femtocellular base stations have certain dynamical power range and transmission powers can be adjusted to suppress the inter-cell interference. Thus, work can be carried forward to include this feature in the future simulator.

In addition, it is also meaningful to investigate the the public safety use case in

downlink aspect. A detached-house case study is also considered to proceed under this framework, which together with the proposed two cases in this thesis, complete the femtocell use study in mobile teletrauma services.

In the long term, the study will continue to reveal the performance of femtocell in the context of LTE, especially with MIMO interface and dynamic spectrum management.

Bibliography

[1] D. Chambers. *Femtocell Primer.* Lulu.com, 2008.

[2] V. Chandrasekhar, J.G. Andrews, and A. Gatherer. Femtocell networks: A survey. *IEEE Communications Magazine*, 46(9):59–67, September 2008.

[3] E. Mutafungwa, Z. Zheng, and J. Hämäläinen. Exploiting femtocellular networks for emergency telemedicine applications in multiple dwelling units. Submitted to 1st International ICST Conference on Public Safety Communication, 2009.

[4] K.S. Gilhousen, I.M. Jacobs, R. Padovani, A.J. Viterbi, Jr. Weaver, L.A., and III Wheatley, C.E. On the capacity of a cellular CDMA system. *Vehicular Technology, IEEE Transactions on*, 40(2):303–312, May 1991.

[5] H. Holma and A. Toskala. *WCDMA for UMTS: HSPA Evolution and LTE.* John Wiley & Sons, Inc., New York, NY, USA, 2007.

[6] 3GPP. Spreading and modulation (FDD). Technical Specification TS 25.213, September 2008.

[7] T. Juhana and Maiyusril. *Information Networking*, chapter UMTS implementation planning on GSM network, pages 614–622. Springer Berlin / Heidelberg, 2003.

[8] 3GPP. Radio interface protocol architecture. Technical Specification TS 25.301, September 2008.

[9] 3GPP. Services provided by the physical layer. Technical Specification TS 25.302, September 2008.

[10] 3GPP. Medium Access Control (MAC) protocol specification. Technical Specification TS 25.321, September 2008.

[11] 3GPP. Radio Link Control (RLC) protocol specification. Technical Specification TS 25.322, September 2008.

[12] 3GPP. Radio Resource Control (RRC); Protocol specification. Technical Specification TS 25.331, September 2008.

[13] 3GPP. High Speed Packet Access (HSPA) evolution; Frequency Division Duplex (FDD). Technical Report TR 25.999, March 2008.

[14] R. Martin. 3G home base stations: Femto cells & FMC for the masses. *Unstrung Insider*, 6, January 2007.

[15] 3GPP. UTRAN architecture for 3G Home NodeB. Technical Specification TS 25.467, December 2008.

[16] 3GPP. FDD Home NodeB RF requirements. Technical Report TR 25.967, April 2009.

[17] 3GPP. Security of H(e)NB. Technical Report TR 33.820, March 2009.

[18] M. Al-Akaidi, D. Alnsour, and O. Alani. Spectral efficiency evaluation in cellular systems. In *3G Mobile Communication Technologies, 2002. Third International Conference on (Conf. Publ. No. 489)*, pages 539–543, May 2002.

[19] M. Husso, J. Hämäläinen, R. Jäntti, and A.M. Wyglinski. Adaptive antennas and dynamic spectrum management for femtocellular networks: A case study. In *New Frontiers in Dynamic Spectrum Access Networks, 2008. DySPAN 2008. 3rd IEEE Symposium on*, pages 1–5, October 2008.

[20] 3GPP. 3G Home NodeB Study Item Technical Report. Technical Report TR 25.820, September 2008.

[21] M. Husso, J. Hämäläinen, R. Jäntti, J. Li, E. Mutafungwa, R. Wichman, and Z. Zheng. Interference suppression by practical transmit beamforming methods in closed femtocells. Submitted to EURASIP Journal on Wireless Communications and Networking, 2009.

[22] H. Claussen. Performance of macro- and co-channel femtocells in a hierarchical cell structure. In *Personal, Indoor and Mobile Radio Communications, 2007. PIMRC 2007. IEEE 18th International Symposium on*, pages 1–5, September 2007.

[23] H. Claussen, L.T.W. Ho, and L.G. Samuel. Self-optimization of coverage for femtocell deployments. In *Wireless Telecommunications Symposium, 2008. WTS 2008*, pages 278–285, April 2008.

[24] H. Claussen and F. Pivit. Femtocell coverage optimization using switched multi-element antennas. In *Communications, 2009. ICC '09. IEEE International Conference on*, pages 1–6, June 2009.

[25] Helsinki City Urban Facts Office. Statistical yearbook of the city of helsinki 2007. City of helsinki urban facts, Statistics and information services, 2007.

[26] C.F.M. Weston, W.J. Penny, and D.G. Julian. Guidelines for the early management of patients with myocardial infarction, 1994.

[27] Jr. Sluyter, A.J.J. The role of communication systems in emergency medical services. *Vehicular Technology, IEEE Transactions on*, 25(4):175–186, November 1976.

[28] H.P.A. Ketterling. *Introduction to Digital Professional Mobile Radio.* Artech House Publishers, 2004.

[29] T.T. Radio. Voice plus data (V+D); part 2: Air interface (AI). *ETSI, EN*, 300:392–2, 2001.

[30] Y. Chu and A. Ganz. A mobile teletrauma system using 3G networks. *Information Technology in Biomedicine, IEEE Transactions on*, 8(4):456–462, December 2004.

[31] 3GPP. Services and service capabilities. Technical Specification TS 22.105, June 2007.

[32] 3GPP. HNB and HNB-Macro Propagation Models. Contribution R4 071617, October 2007.

[33] 3GPP. Text Proposal for 36.814 on the Relay-to-UE Channel Model. Contribution R1 091567, 2009.

[34] 3GPP. Evolved Universal Terrestrial Radio Access (E-UTRA); Physical channels and modulation. Technical Specification TS 36.211, September 2008.

[35] 3GPP. Physical layer procedures (FDD). Technical Specification TS 25.214, September 2008.

[36] A.A. Dowhuszko, G. Corral-Briones, J. Hämäläinen, and R. Wichman. Achievable sum-rate analysis of practical multiuser scheduling schemes with limited feedback. In *Communications, 2007. ICC '07. IEEE International Conference on*, pages 4381–4386, June 2007.

[37] A.A. Dowhuszko, G. Corral-Briones, J. Hämäläinen, and R. Wichman. On throughput-fairness tradeoff in virtual MIMO systems with limited feedback. *Wireless Communications and Networking, EURASIP Journal on*, 2009(102064), 2009.

[38] A. Papoulis and S.U. Pillai. *Probability, Random Variables and Stochastic Processes.* McGraw-Hill Education (India) Pvt Ltd, 2002.

[39] P. Mogensen, Wei Na, I.Z. Kovacs, F. Frederiksen, A. Pokhariyal, K.I. Pedersen, T. Kolding, K. Hugl, and M. Kuusela. LTE capacity compared to the shannon bound. In *Vehicular Technology Conference, 2007. VTC2007-Spring. IEEE 65th*, pages 1234–1238, April 2007.

[40] M. Abramowitz and I.A. Stegun. *Handbook of Mathematical Functions with Formulas, Graphs, and Mathematical Table.* Courier Dover Publications, 1965.